

# Disentangling Long-Short Term State Under Unknown Interventions for Online Time Series Forecasting

Ruichu Cai<sup>1, 2</sup>, Haiqin Huang<sup>1</sup>, Zhifan Jiang<sup>1</sup>, Zijian Li<sup>3\*</sup>, Changze Zhou<sup>1</sup>,  
Yuequn Liu<sup>1</sup>, Yuming Liu<sup>1</sup>, Zhifeng Hao<sup>4</sup>

<sup>1</sup>School of Computer Science, Guangdong University of Technology, China

<sup>2</sup>Peng Cheng Laboratory, Shenzhen, China

<sup>3</sup>Machine Learning Department, Mohamed bin Zayed University of Artificial Intelligence, United Arab Emirates

<sup>4</sup>Shantou University

## Abstract

Current methods for time series forecasting struggle in the online scenario, since it is difficult to preserve long-term dependency while adapting short-term changes when data are arriving sequentially. Although some recent methods solve this problem by controlling the updates of latent states, they cannot disentangle the long/short-term states, leading to the inability to effectively adapt to nonstationary. To tackle this challenge, we propose a general framework to disentangle long/short-term states for online time series forecasting. Our idea is inspired by the observations where short-term changes can be led by unknown interventions like abrupt policies in the stock market. Based on this insight, we formalize a data generation process with unknown interventions on short-term states. Under mild assumptions, we further leverage the independence of short-term states led by unknown interventions to establish the identification theory to achieve the disentanglement of long/short-term states. Built on this theory, we develop a **Long Short-Term Disentanglement model (LSTD)** to extract the long/short-term states with long/short term encoders, respectively. Furthermore, the **LSTD** model incorporates a smooth constraint to preserve the long-term dependencies and an interrupted dependency constraint to enforce the forgetting of short-term dependencies, together boosting the disentanglement of long/short-term states. Experimental results on several benchmark datasets show that our **LSTD** model outperforms existing methods for online time series forecasting, validating its efficacy in real-world applications.

Code — <https://github.com/DMIRLAB-Group/LSTD>

## Introduction

As one of the most fundamental tasks in time series analysis (Hamilton 2020; Liu et al. 2023b), time series forecasting (Zhou et al. 2021; Zeng et al. 2023; Kitaev, Kaiser, and Levskaya 2020; Liu et al. 2021; Wu et al. 2021; Zhou et al. 2021) plays a critical role in various fields such as finance (Clements, Franses, and Swanson 2004; Cao, Li, and Li 2019), and traffic (Lippi, Bertini, and Frasconi 2013). However, in the industry, since time series data often arrives sequentially and is accompanied by temporal distribu-

tion shifts (Wang et al. 2022; Li et al. 2024b), existing methods (Wu et al. 2021; Nie et al. 2022; Lopez-Paz and Ranzato 2017) that heavily rely on the mini-batch training paradigm can hardly adapt to these changing distributions, leading to suboptimal prediction results in the online scenario.

To solve this problem, several recent methodologies (Cai et al. 2023; Guo et al. 2024; Mejri, Amarnath, and Chatterjee 2024; Lin 1992) are proposed to adapt the short-term nonstationarity and long-term dependencies. FSNet (Pham et al. 2022) leverages the partial derivative to characterize the short-term information and an associative memory to preserve the long-term dependencies. To better combine long-term and short-term historical information, OneNet (Wen et al. 2024) uses a reinforcement learning-based to dynamically adjust the combination of temporal correlation and cross-variable dependency models. Recently, Zhang et al. (Zhang et al. 2024b) propose the Concept Drift Detection and Adaptation framework (D<sup>3</sup>A), which first detects the temporal distribution shift and then employs an aggressive manner to update the model. In summary, these methods aim to address online time series forecasting via two steps: 1) disentangling long/short-term states; and 2) adapting short-term states and reusing long-term states for forecasting. Please refer to Appendix A for further discussion about online time series forecasting and causal representation learning.

Although current methods achieve non-trivial contributions on how to update short-term states or how to efficiently combine the long/short-term states, they implicitly assume that the long/short-term states have been well-disentangled from nonstationary time series data. However, this assumption is hard to meet, and without disentanglement of the long/short-term states, existing methods can hardly adapt to the nonstationary environments. Figure 1 provides a finance example, where the monetary exchange rate is influenced by the short-term variables (e.g. customs duties) and the long-term variables (e.g., financial revenue). Nonstationarity occurs due to unknown customs tariff policies. As shown in Figure 1 (a), when the long-term and short-term latent variables are not disentangled, the financial revenues are entangled with the customs duties. As a result, existing methods can be hard to effectively adapt to the changes in financial revenues and may obtain an inaccurate forecasting perfor-

\*corresponding author: Zijian Li (leizigin@gmail.com)  
Copyright © 2025, Association for the Advancement of Artificial Intelligence (www.aaai.org). All rights reserved.

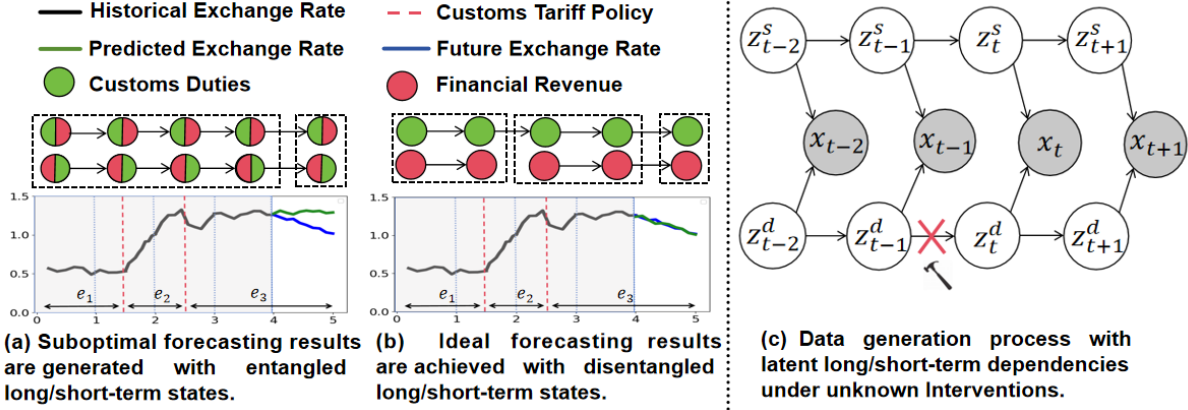


Figure 1: Illustration of sequentially arriving exchange rate data, which is influenced by short-term customs duties and long-term financial revenue. Moreover, the short-term customs duties are intervened by sudden customs tariff policies. (a) If the estimated short-term customs duties and long-term financial revenue are entangled, short-term influence from Environments (e.g.,  $e_1, e_2, e_3$ ) may affect the effectiveness of the models to adapt to the changing environments, leading to suboptimal forecasting performance. (b) When the long/short-term states are disentangled, the model can quickly adapt to environmental changes and hence achieve correct forecasting results. (c) Data generation process for time-series data.  $z_t^s$  and  $z_t^d$  denotes the long/short-term states. Note that the short-term states  $z_t^d$  are intervened randomly.

mance even if they use a masterly strategy to update the short-term states and preserve the long-term states.

Based on the aforementioned example, we observe that nonstationarity is brought by the unknown interventions on short-term states. Moreover, to address the online forecasting task, it is intuitive to find that we should disentangle the long/short-term states from the time series with unknown interventions as shown in Figure 1 (b). Under this intuition, we first consider that the sequentially arriving data follow a data generation process in Figure 1 (c), where the latent short-term states are influenced by unknown interventions. Under mild assumptions, we establish disentanglement results on long/short-term states by leveraging the independence of intervened short-term states. To bridge the gap between theory and practice, we further develop a **Long Short-Term Disentanglement model (LSTD)** to solve the online time series forecasting problem. Specifically, the proposed **LSTD** model includes a minimal update constraint to preserve the long-term dependencies and an interrupted dependency constraint to enforce the forgetting of short-term dependencies, which facilitates the disentanglement of long-term and short-term latent states. Empirical results on several real-world benchmark datasets show that the proposed **LSTD** method outperforms existing state-of-the-art methods for online time series forecasting, highlighting its effectiveness in real-world applications.

## Data Generation Process for Time Series Data

To show how to disentangle the long-term and short-term latent states in the online time series forecasting scenario, we first introduce the data generation process of time series data as shown in Figure 1 (c). Mathematically, we let  $\mathbf{x} = \{\mathbf{x}_1, \mathbf{x}_2, \dots, \mathbf{x}_t, \dots\}$  be time series data with discrete time steps, in which each observation  $\mathbf{x}_t$  is generated from

latent variables  $\mathbf{z}_t$  through an invertible and nonlinear mixing function  $g$  as formalized in Equation (1).

$$\mathbf{x}_t = g(\mathbf{z}_t). \quad (1)$$

At each time step  $t$ ,  $\mathbf{z}_t \in \mathbb{R}^n$  are divided into the long-term latent states  $\mathbf{z}_t^s \in \mathbb{R}^{n_s}$  and short-term latent states  $\mathbf{z}_t^d \in \mathbb{R}^{n_d}$ , and  $n = n_s + n_d$ . Moreover, the  $i$ -th component of  $\mathbf{z}_t^s$  is generated by some components of historical long-term latent states  $\mathbf{z}_{t-\tau}^s$  with the time lag of  $\tau$  via a nonparametric function as shown in Equation (2).

$$z_{t,i}^s = f_i^s(\{z_{t-\tau,k}^s | z_{t-\tau,k}^s \in \mathbf{Pa}(z_{t,i}^s)\}, \varepsilon_{t,i}^s), \quad (2)$$

with  $\varepsilon_{t,i}^s \sim p_{\varepsilon_{t,i}^s}$ ,

where  $\mathbf{Pa}(z_{t,i}^s)$  denotes the set of latent variables that directly cause  $z_{t,i}^s$  and  $\varepsilon_{t,i}^s$  denotes the temporally and spatially independent noise extracted from a distribution  $p_{\varepsilon_{t,i}^s}$ .

Moreover, according to the observation in the example in Figure 1, we assume that the nonstationarity in time series data is led by the interventions on the short-term latent variables (e.g., the truncation between  $\mathbf{z}_{t-1}^d$  and  $\mathbf{z}_t^d$  in Figure 1 (c)). It is noted that when the interventions occur is unknown. To illustrate the randomness of the interventions, we let  $I$  be an indicator to decide if an intervention occurs and  $I$  comes from a Bernoulli distribution  $\mathbf{B}(I, \theta)$  with the probability of  $\theta$ . When  $I = 0$ , it indicates no intervention, whereas when  $I = 1$ , it signifies intervention. When intervention occurs, the data is generated solely by noise. Formally, the generation process of the short-term latent variables is shown as follows:

$$z_{t,j}^d = \begin{cases} f_j^d(\{z_{t-\tau,k}^d | z_{t-\tau,k}^d \in \mathbf{Pa}(z_{t,j}^d)\}, \varepsilon_{t,j}^d) & , \text{if } I = 0 \\ f_j^d(\varepsilon_{t,j}^d) & , \text{if } I = 1 \end{cases}$$

where  $\varepsilon_{t,j}^d \sim p_{\varepsilon_{t,j}^d}$  and  $I \sim \mathbf{B}(I, \theta)$ , (3)

where  $\mathbf{Pa}(z_{t,j}^d)$  denotes the set of latent variables that directly cause  $z_{t,j}^d$  and  $\varepsilon_{t,j}^d$  denotes the temporally and spatially independent noise extracted from a distribution  $p_{\varepsilon_{t,j}^d}$ .

The data generation process as shown in Equation (1)-(3) can be well interpreted by the aforementioned financial example. First, the exchange rate can be considered as the observation time series data. Sequentially, the financial revenue and the customs duties denote the long-term and short-term latent variables, respectively. Finally,  $I = 1$  denotes that the customs tariff policy intervenes with customs duties and leads to temporal distribution changes. In the context of online time series forecasting, where the time series data arrive sequentially, we first predict the value of  $\mathbf{x}_{L+1:H}$  given  $\mathbf{x}_{1:L}$  at  $t$ -th time step. Then at  $t+1$ -th time step, we have access to the true value of  $\mathbf{x}_{L+1:H}$  to update the model and then use  $\mathbf{x}_{2:L+1}$  to predict the value of  $\mathbf{x}_{L+2:H+1}$ .

## Disentanglement of Long-Term and Short-Term States

To disentangle the long-term latent variables  $\mathbf{z}_t^s$  and the short-term latent variables  $\mathbf{z}_t^d$ , we propose the block-wise identification theory in Theory 1. Mathematically, the block-wise identification means that for the ground-truth  $\mathbf{z}_t^*$ , there exists  $\hat{\mathbf{z}}_t^*$  and an invertible function  $h_z^* : \mathbb{R}^{n^*} \rightarrow \mathbb{R}^{n^*}$ , such that  $\hat{\mathbf{z}}_t^* = h_z^*(\mathbf{z}_t^*)$ . And  $*$  can be  $d$  or  $s$ .

**Theorem 1. (Subspace Identification of the long-term and short-term Latent Variables)** Suppose that the observed data from long/short-term is generated following the data generation process in Figure 1 (c), and we further make the following assumptions:

- **A1 (Smooth, Positive and Conditional independent Density:)** (Yao, Chen, and Zhang 2022; Yao et al. 2021) The probability density function of latent variables is smooth and positive, i.e.,  $p(\mathbf{z}_{t-\tau+1:t} | \mathbf{z}_{t-\tau}) > 0$  over  $\mathbf{Z}_{t-\tau}$  and  $\mathbf{Z}_{t-\tau+1:t}$ . Conditioned on  $\mathbf{z}_{t-\tau}$  each  $z_i$  is independent of any other  $z_j$  for  $i, j \in 1, \dots, n, i \neq j$ , i.e.,  $\log p(\mathbf{z}_{t-\tau+1:t} | \mathbf{z}_{t-\tau}) = \sum_{k=1}^{n_s} \log p(z_{t-\tau+1:t,k} | \mathbf{z}_{t-\tau})$
- **A2 (non-singular Jacobian):** (Kong et al. 2023b) Each generating function  $g$  has non-singular Jacobian matrices almost anywhere and  $g$  is invertible.
- **A3 (Linear Independence:)** (Yao, Chen, and Zhang 2022) For any  $\mathbf{z}^d \in \mathbf{Z}_{t-\tau+1:t}^d \subseteq \mathbb{R}^{n_d}$ ,  $\bar{v}_{t-\tau,1}, \dots, \bar{v}_{t-\tau,n_d}$  as  $n_d$  vector functions in  $z_{t-\tau,1}^d, \dots, z_{t-\tau,l}^d, \dots, z_{t-\tau,n_d}^d$  are linear independent, where  $\bar{v}_{t-\tau,l}$  are formalized as follows:

$$\bar{v}_{t-\tau,l} = \frac{\partial^2 \log p(\mathbf{z}_{t-\tau+1:t}^d | \mathbf{z}_{t-\tau}^d)}{\partial z_{t-\tau+1:t,k}^d \partial z_{t-\tau,l}^d} \quad (4)$$

Suppose that we learn  $(\hat{g}, \hat{f}_i^s, \hat{f}_i^d)$  to achieve Equation (1)-(3) with the minimal number of transition edge among short term latent variables  $\mathbf{z}_1^d, \dots, \mathbf{z}_t^d, \dots$ , then the long-term and short-term latent variables are block-wise identifiable.

**Proof Sketch:** The proof can be found in Appendix B. First, we construct an invertible transformation  $h_z$  between the ground-truth latent variables and estimated ones. Sequentially, we prove that the ground truth of long-term latent

variables is not the function of short-term latent variables by leveraging the pairing time series from different influences. Sequentially, we leverage sufficient variability of historical information to show that the short-term latent variables are not the function of the estimated long-term latent variables. Moreover, by leveraging the invertibility of transformation  $h_z$ , we can obtain the Jacobian of  $h_z$  as shown in Equation (B.36), where  $B = 0$  and  $C = 0$ , since the ground truth long-term latent variables are not the functions of short-term latent variables and the short-term latent variables are not the function of the estimated long-term latent variables.

$$\mathbf{J}_{h_z} = \left[ \begin{array}{c|c} \mathbf{A} := \frac{\partial \mathbf{z}_t^s}{\partial \hat{\mathbf{z}}_t^s} & \mathbf{B} := \frac{\partial \mathbf{z}_t^s}{\partial \hat{\mathbf{z}}_t^d} = 0 \\ \hline \mathbf{C} := \frac{\partial \mathbf{z}_t^d}{\partial \hat{\mathbf{z}}_t^s} = 0 & \mathbf{D} := \frac{\partial \mathbf{z}_t^d}{\partial \hat{\mathbf{z}}_t^d} \end{array} \right] \quad (5)$$

**Discussion of the Identification Results:** We would like to highlight that the theoretical results provide sufficient conditions for the identification of our model. That implies: 1) our model can be correctly identified when all the assumptions hold. 2) at the same time, even if some of the above assumptions do not hold, our method may still learn the correct model. From an application perspective, these assumptions rigorously defined a subset of applicable scenarios of our model. Thus, we provide detailed explanations of the assumptions, how they relate to real-world scenarios, and in which scenarios they are satisfied.

**Smooth, Positive and Conditional independent Density.** This assumption is common in the existing identification results (Yao, Chen, and Zhang 2022; Yao et al. 2021; Yao, Chen, and Zhang 2022; Yao et al. 2021). In real-world scenarios, smooth and positive density implies continuous changes in historical information, such as temperature variations in weather data. To achieve this, we should sample as much data as possible to learn the transition probabilities more accurately. Moreover, The conditional independent assumption is also common in identifying temporal latent processes (Li et al. 2024a). Intuitively, it means there are no immediate relations among latent variables. To satisfy this assumption, we can sample data at high frequency to avoid instantaneous dependencies caused by subsampling.

**Non-singular Jacobian of  $g$ .** This assumption is also common in (Kong et al. 2023b; Li et al. 2024b,c; Xie et al. 2023; Kong et al. 2023a). Mathematically, it denotes that the Jacobian from the latent variables to the observed variables is full rank. In real-world scenarios, it means that there is at least one observation for each latent variable. To meet this assumption, we can ignore such independent latent variables since they have no influence on the observations.

## Linear Independence.

**Data generation process with unknown interventions.** In real-world time series data, there are many unknown interventions that lead to nonstationarity like the financial example in Figure 1. Therefore, this assumption is reasonable. Besides, we need to impose discontinuities in the short-term components to break the symmetry between the long and short terms in the causal graph. This ensures that the long

and short terms are identifiable. Through the identifiable theory, we can explain whether the module learns long-term or short-term components, thereby theoretically guaranteeing the disentanglement of long and short terms. In practice, we may investigate the nonstationarity of the data to test whether this assumption is valid.

## Long Short-Term Disentanglement Model Model Overview

In this section, we introduce the implementation of the long/short-term disentanglement model as shown in Figure 2. Specifically, it uses a variational sequential autoencoder as a backbone architecture and further employs long-term and short-term prior architectures with smooth constraint and sparse dependency constraint for long-term and short-term latent variable disentanglement.

### Variational Sequential Autoencoder

To model the time series data, we follow the data generation process in Figure 1 (c) and derive the evidence lower bound (ELBO) as shown in Equation (6).

$$ELBO = \underbrace{\mathbb{E}_{q(\mathbf{z}_{1:H}^s | \mathbf{x}_{1:H})} \mathbb{E}_{q(\mathbf{z}_{1:H}^d | \mathbf{x}_{1:H})} \ln p(\mathbf{x}_{1:H} | \mathbf{z}_{1:H}^s, \mathbf{z}_{1:H}^d)}_{L_R + L_P} - \underbrace{D_{KL}(q(\mathbf{z}_{1:H}^s | \mathbf{x}_{1:H}) || p(\mathbf{z}_{1:H}^s))}_{L_K^s} - \underbrace{D_{KL}(q(\mathbf{z}_{1:H}^d | \mathbf{x}_{1:H}) || p(\mathbf{z}_{1:H}^d))}_{L_K^d} \quad (6)$$

where  $L_R$  and  $L_P$  denote the reconstructed and prediction loss, respectively:

$$L_R = \frac{1}{L} \sum_{i=1}^L (\hat{\mathbf{z}}_i - \mathbf{z}_i)^2 \quad (7)$$

$$L_P = \frac{1}{H-L} \sum_{i=L+1}^H (\hat{\mathbf{z}}_i - \mathbf{z}_i)^2$$

$D_{KL}$  denotes the KL divergence. Specifically,  $q(\mathbf{z}_{1:H}^s | \mathbf{x}_{1:H})$ ,  $q(\mathbf{z}_{1:H}^d | \mathbf{x}_{1:H})$ , which includes the encoder and the latent transition module in Figure 2, is used to approximate the prior distribution.  $p(\mathbf{x}_{1:H} | \mathbf{z}_{1:H}^s, \mathbf{z}_{1:H}^d)$  is used to reconstruct the historical observations and forecast the future values. The aforementioned two distributions can be formalized as follows:

$$\hat{\mathbf{z}}_{1:H}^s, \hat{\mathbf{z}}_{1:H}^d = \phi(\mathbf{x}_{1:H}), \quad \hat{\mathbf{x}}_{1:H} = \psi(\mathbf{z}_{1:H}), \quad (8)$$

Where  $\mathbf{z}_{1:H}$  denotes the combination of  $\hat{\mathbf{z}}_{1:H}^s$  and  $\hat{\mathbf{z}}_{1:H}^d$ . For the implementation of  $\phi$ , we follow the backbone of FSNet (Pham et al. 2022). For the implementation of  $\psi$ , we employ an MLP (Multilayer Perceptron). Please refer to Appendix C for more implementation details of the **LSTD** model.

### Long-Term and Short-Term Prior Networks

To model the prior distribution of the long-term latent variables, we propose the long-term prior networks. Similar to

the existing methods for causal representation learning (Yao et al. 2021; Yao, Chen, and Zhang 2022), we let  $\{r_i^s\}$  be a set of learned inverse transition functions that take the estimated long-term latent variables and output the noise term, i.e.,  $\hat{e}_{t,i}^s = r_i^s(\hat{z}_{t,i}^s, \hat{z}_{t-1}^s)$ <sup>1</sup> and each  $r_i^s$  is modeled with MLPs. Then we devise a transformation  $\kappa^s := \{\hat{\mathbf{z}}_{t-1}^s, \hat{\mathbf{z}}_t^s\} \rightarrow \{\hat{\mathbf{z}}_{t-1}^s, \hat{e}_t^s\}$ , and its Jacobian is  $\mathbf{J}_{\kappa^s} = \begin{pmatrix} \mathbb{I} & 0 \\ M & \text{diag}\left(\frac{\partial r_i^s}{\partial \hat{z}_{t,i}^s}\right) \end{pmatrix}$ , where  $M$  denotes a matrix. By applying the change of variables formula, we have the following equation:

$$\log p(\hat{\mathbf{z}}_{t-1}^s, \hat{\mathbf{z}}_t^s) = \log p(\hat{\mathbf{z}}_{t-1}^s, \hat{e}_t^s) + \log |\det(\mathbf{J}_{\kappa^s})|. \quad (9)$$

Since we assume that the noise term in Equation (9) is independent with  $\mathbf{z}_{t-1}^s$ , we can enforce the independence of the estimated noise  $\hat{e}_t^s$  and further have:

$$\log p(\hat{\mathbf{z}}_t^s | \hat{\mathbf{z}}_{t-1}^s) = \log p(\hat{e}_t^s) + \sum_{i=1}^{n_s} \log \left| \frac{\partial r_i^s}{\partial \hat{z}_{t,i}^s} \right|. \quad (10)$$

Therefore, the long-term prior can be estimated as follows:

$$\log p(\mathbf{z}_{1:t}^s) = \log p(\hat{\mathbf{z}}_1^s) + \sum_{\tau=2}^t \left( \sum_{i=1}^{n_s} \log p(\hat{e}_{\tau,i}^s) + \sum_{i=1}^{n_s} \log \left| \frac{\partial r_i^s}{\partial \hat{z}_{\tau,i}^s} \right| \right), \quad (11)$$

where  $p(\hat{e}_i^s)$  follow Gaussian distributions. Similarly, we can further estimate the short-term prior as follows:

$$\log p(\mathbf{z}_{1:t}^d) = \log p(\hat{\mathbf{z}}_1^d) + \sum_{\tau=2}^t \left( \sum_{i=1}^{n_d} \log p(\hat{e}_{\tau,i}^d) + \sum_{i=1}^{n_d} \log \left| \frac{\partial r_i^d}{\partial \hat{z}_{\tau,i}^d} \right| \right), \quad (12)$$

### Smooth Constraint for Long-Term Disentanglement

To preserve the long-term dependencies in the long-term latent variables, we propose the smooth constraint. Since the causal relationships of the long-term dependencies are stable, the association of the long-term dependencies is also stable. Based on this insight, we consider the attention weights as associations and extract the association with the help of the self-attention mechanism. Specifically, we first split the  $\mathbf{z}_{1:H}^s$  into two equal-size segmentation  $\mathbf{z}_{1:H/2}^s$  and  $\mathbf{z}_{H/2:H}^s$ . And then the association of  $\mathbf{z}_{1:H/2}^s$  and  $\mathbf{z}_{H/2:H}^s$  can be formalized as follows:

$$A_{\mathbf{z}_h^s} = \text{Softmax}\left(\frac{\mathbf{z}_{1:H/2}^s \mathbf{z}_{1:H/2}^s^\top}{\sqrt{n_s}}\right), \quad (13)$$

$$A_{\mathbf{z}_e^s} = \text{Softmax}\left(\frac{\mathbf{z}_{H/2:H}^s \mathbf{z}_{H/2:H}^s^\top}{\sqrt{n_s}}\right),$$

in which  $A_{\mathbf{z}_h^s}$  and  $A_{\mathbf{z}_e^s}$  denote the association matrices of the start half and the end half segments. Hence, we can restrict the long-term dependencies by restricting the similarity of these two matrices as shown in Equation (14)

$$\mathcal{L}_m = \|A_{\mathbf{z}_h^s} - A_{\mathbf{z}_e^s}\|_2, \quad (14)$$

where  $\|\cdot\|_2$  denotes the L2 norm of matrices.

<sup>1</sup>We use the superscript symbol to denote estimated variables.

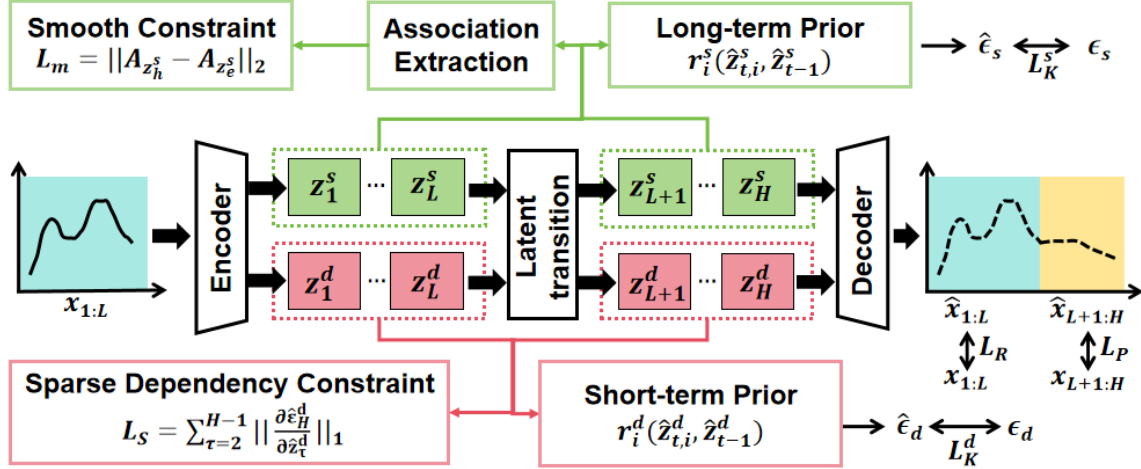


Figure 2: The framework of the proposed **LSTD** model. The long/short-term latent variables  $z_{1:L}^d$  and  $z_{1:L}^s$  are extracted from the encoder. And the latent transition module is used to estimated the  $z_{L+1:H}^d$  and the  $z_{L+1:H}^s$  from  $z_{1:L}^d$  and  $z_{1:L}^s$ , respectively. The long-term and short-term prior networks are used to estimate the prior distributions.

### Interrupted Dependency Constraint for Short-Term Disentanglement

Since the nonstationarity is assumed to be led by the interventions to the short-term latent variables, given  $z_{1:H}^d$ , if intervention occurs at  $\tau$ -th time step, and  $2 < \tau < H-1$ , then  $\frac{\partial \hat{z}_{\tau-1}^d}{\partial z_{\tau-1}^d} = 0$ , where  $i, j \in \{1, \dots, n_d\}$ . Based on this intuition, we aim to enforce the interruption of the estimated short-term dependencies to meet the unknown interventions. To achieve this, we propose the interrupted dependency constraint for the short-term variables. Specifically, given the estimated short-term variables  $z_{1:H}^d$ , we have:

$$\mathcal{L}_s = \sum_{(i,j) \in \{1, \dots, n_d\}} \sum_{\tau \in \{2, \dots, H-1\}} \left\| \frac{\partial \hat{z}_{\tau-1}^d}{\partial z_{\tau-1}^d} \right\|_1, \quad (15)$$

where  $\|\cdot\|_1$  denote the L1 norm.

By using the aforementioned interrupted dependency constraint, the intervention on the short-term latent variables can be automatically detected, which finally enforces the disentanglement of the short-term latent variables.

### Model Summary

By combining the aforementioned variational sequentially autoencoder with the restriction of smooth constraint and interrupted dependency constraint, we can finally formalize the total loss of the proposed **LSTD** model as follows:

$$\mathcal{L} = L_R + L_P + \beta L_K + \alpha L_m + \gamma L_s, \quad (16)$$

where  $L_K = L_K^s + L_K^d$ . And  $\alpha, \beta, \gamma$  are hyper-parameters.

## Experiment

### Datasets

To evaluate the performance of our method, we consider the following datasets. **ETT** is an electricity transformer temperature dataset collected from two separate

counties in China, which contains two separate datasets  $\{\text{ETTh2}, \text{ETTm1}\}$  for one hour level and minutes level, respectively. **Exchange** is the daily exchange rate dataset from eight foreign countries including Australia, British, Canada, Switzerland, China, Japan, New Zealand, and Singapore ranging from 1990 to 2016. **Weather**<sup>2</sup> is recorded at the Weather Station at the Max Planck Institute for Biogeochemistry in Jena, Germany. **ECL**<sup>3</sup> is an electricity-consuming load dataset with the electricity consumption (kWh) collected from 321 clients. **Traffic**<sup>4</sup> is a dataset of traffic speeds collected from the California Transportation Agencies (CalTrans) Performance Measurement System (PeMS). For each dataset, we follow the standard pre-processing and setting in OneNet (Wen et al. 2024).

### Baselines

We consider nine state-of-the-art as follows: OneNet (Wen et al. 2024) which considered the temporal and feature relationships and used reinforcement learning to update their relationships in real-time. At the same time, we compared with a very excellent backbone model FSNet (Pham et al. 2022) which considered gradient updates to optimize fast new as well as retained information and be used in OneNet. Besides, we also compared the OneNet model with TCN as its backbone named OneNet-TCN, and the regular usage of TCN named Online-TCN (Zinkevich 2003) for online learning. The Experience Replay (ER) (Chaudhry et al. 2019) stored the previous data in a buffer and interleaved with newer samples during learning. Meanwhile, ER has many advanced variants: TFCL (Aljundi, Kelchtermans, and Tuytelaars 2019) used a task-boundary detection mechanism and a knowledge consolidation strategy; MIR (Aljundi et al.

<sup>2</sup><https://www.bgc-jena.mpg.de/wetter/>

<sup>3</sup><https://archive.ics.uci.edu/dataset/321/electricityloaddiagrams20112014>

<sup>4</sup><https://pems.dot.ca.gov/>

Models	Len	LSTD	OneNet	FSNet	OneNet-T	DER++	ER	MIR	TFCL	Online-T	Informer
ETTh2	1	<b>0.377</b>	0.380	0.466	0.411	0.508	0.508	0.486	0.557	0.502	7.571
	24	0.543	<b>0.532</b>	0.687	0.772	0.828	0.808	0.812	0.846	0.830	4.629
	48	0.616	<b>0.609</b>	0.846	0.806	1.157	1.136	1.103	1.208	1.183	5.692
ETTm1	1	<b>0.081</b>	0.082	0.085	0.082	0.083	0.086	0.085	0.087	0.214	0.456
	24	0.102	<b>0.098</b>	0.115	0.212	0.196	0.202	0.192	0.211	0.258	0.478
	48	0.115	<b>0.108</b>	0.127	0.223	0.208	0.220	0.210	0.236	0.283	0.388
WTH	1	<b>0.153</b>	0.156	0.162	0.171	0.174	0.180	0.179	0.177	0.206	0.426
	24	<b>0.136</b>	0.175	0.188	0.293	0.287	0.293	0.291	0.301	0.308	0.380
	48	<b>0.157</b>	0.200	0.223	0.310	0.294	0.297	0.297	0.323	0.302	0.367
ECL	1	<b>2.112</b>	2.351	3.143	2.470	2.657	2.579	2.575	2.732	3.309	3.813
	24	<b>1.422</b>	2.074	6.051	4.713	8.996	9.327	9.265	12.094	11.339	9.185
	48	<b>1.411</b>	2.201	7.034	4.567	9.009	9.685	9.411	12.110	11.534	11.183
Traffic	1	<b>0.231</b>	0.241	0.312	0.236	0.271	0.284	0.298	0.306	0.334	0.234
	24	<b>0.398</b>	0.438	0.426	0.425	0.476	0.461	0.451	0.441	0.481	0.451
	48	<b>0.426</b>	0.473	0.445	0.451	0.486	0.510	0.502	0.438	0.503	0.496
Exchange	1	<b>0.013</b>	0.017	0.094	0.031	0.106	0.097	0.095	0.106	0.113	0.102
	24	<b>0.039</b>	0.047	0.113	0.060	0.111	0.162	0.104	0.098	0.116	0.107
	48	<b>0.043</b>	0.062	0.156	0.065	0.183	0.181	0.101	0.101	0.168	0.116

Table 1: Mean Square Error (MSE) results on the different datasets. TCN is abbreviated as T

2019) selected samples that cause the most forgetting; and DER++ (Buzzega et al. 2020) incorporated a knowledge distillation strategy. Additionally, we have incorporated a long-term time-series forecasting model, Informer (Zhou et al. 2021), to investigate the performance of conventional forecasting models in online time-series forecasting problems.

## Quantitative Results and Discussion

Experiment results on each dataset are shown in Table 1 and Table 2. Since some methods report the best results on the original paper, we also show the best results on the aforementioned tables. Please refer to Appendix D for the experiment results with mean and variance over three random seeds. Our **LSTD** model significantly outperforms all other baselines on most online forecasting tasks. Specifically, our method outperforms the most competitive baselines by a clear margin of 44% on the Exchange, which verifies the example in the introduction. Moreover, our method also greatly reduced prediction errors in the WTH and ECL datasets. However, our method achieves the second-best but still comparable results in the ETT dataset, this might be because there are a few unknown interventions in the ETT datasets. How to address other types of nonstationarity will be an interesting future direction. In addition, we conduct performance analysis experiments and visualization in Appendix D. Compared with other models, we can find that the proposed **LSTD** has the best model performance and relatively good model efficiency.

## Qualitative Results and Discussion

We further conduct visualization results in the WTH and Exchange dataset in Figure 4. Remarkably, our method detects interventions well and achieves better visualization results than that of OneNet and FSNet, which do not explicitly disentangle the short-term and long-term variables. This is because the long/short term variables of these methods might

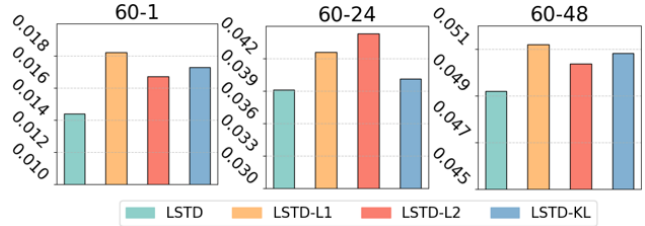


Figure 3: Ablation study on the Exchange datasets. We explore the impact of different loss terms

be entangled, hindering the rapid adaptation to the changing environment of the data streams, and finally resulting in suboptimal predictions. In the meanwhile, our method disentangles the long/short term variables by sparsity dependency constraint, and can efficiently adapt to the new environment. At the same time, the smooth constraint further maintains the long-term variables behind the time series data. Therefore, the prediction curve of our method can well align with the ground truth even if the prediction length is long.

## Ablation Study

We further devise three model variants. a) **LSTD-L1**: we remove the interrupted dependency constraint for short-term disentanglement. b) **LSTD-L2**: we remove the smooth constraint for long-term disentanglement. c) **LSTD-KL**: we remove the long/short-term prior and the corresponding Kullback-Leibler divergence term. Experiment results on the Exchange dataset are shown in Figure 3. We find that 1) the performance of **LSTD-L1** drops without an accurate forgetting of the information, implying that the accurate forgetting benefits the quickly adapting to changes in the data domain and improves the disentanglement and forecasting performance. 2) the performance of **LSTD-L2** drops without re-

Models	Len	LSTD	OneNet	FSNet	OneNet-T	DER++	ER	MIR	TFCL	Online-T	Informer
ETTh2	1	<b>0.347</b>	0.348	0.368	0.374	0.375	0.376	0.410	0.472	0.436	0.850
	24	0.411	<b>0.407</b>	0.467	0.511	0.540	0.543	0.541	0.548	0.547	0.668
	48	<b>0.423</b>	0.436	0.515	0.543	0.577	0.571	0.565	0.592	0.589	0.752
ETTm1	1	<b>0.187</b>	<b>0.187</b>	0.191	0.191	0.192	0.197	0.197	0.198	0.085	0.512
	24	<b>0.217</b>	0.225	0.249	0.319	0.326	0.333	0.325	0.341	0.381	0.525
	48	0.249	<b>0.238</b>	0.263	0.371	0.340	0.351	0.342	0.363	0.403	0.460
WTH	1	<b>0.200</b>	0.201	0.216	0.221	0.235	0.244	0.244	0.240	0.276	0.458
	24	<b>0.223</b>	0.225	0.276	0.345	0.351	0.356	0.355	0.363	0.367	0.417
	48	<b>0.242</b>	0.279	0.301	0.356	0.359	0.363	0.361	0.382	0.362	0.419
ECL	1	<b>0.226</b>	0.254	0.472	0.411	0.421	0.506	0.504	0.524	0.635	0.549
	24	<b>0.292</b>	0.333	0.997	0.513	1.035	1.057	1.066	1.256	1.196	1.198
	48	<b>0.294</b>	0.348	1.061	0.534	1.048	1.074	1.079	1.303	1.235	1.164
Traffic	1	<b>0.225</b>	0.240	0.278	0.236	0.251	0.256	0.284	0.297	0.284	0.258
	24	<b>0.316</b>	0.346	0.365	0.346	0.409	0.417	0.443	0.493	0.385	0.365
	48	<b>0.332</b>	0.371	0.378	0.355	0.386	0.294	0.397	0.531	0.380	0.394
Exchange	1	<b>0.070</b>	0.085	0.174	0.117	0.173	0.124	0.118	0.153	0.169	0.115
	24	<b>0.132</b>	0.148	0.206	0.166	0.227	0.210	0.204	0.227	0.213	0.196
	48	<b>0.142</b>	0.170	0.254	0.173	0.243	0.241	0.209	0.183	0.258	0.217

Table 2: Mean Absolute Error (MAE) results on the different datasets. TCN is abbreviated as T

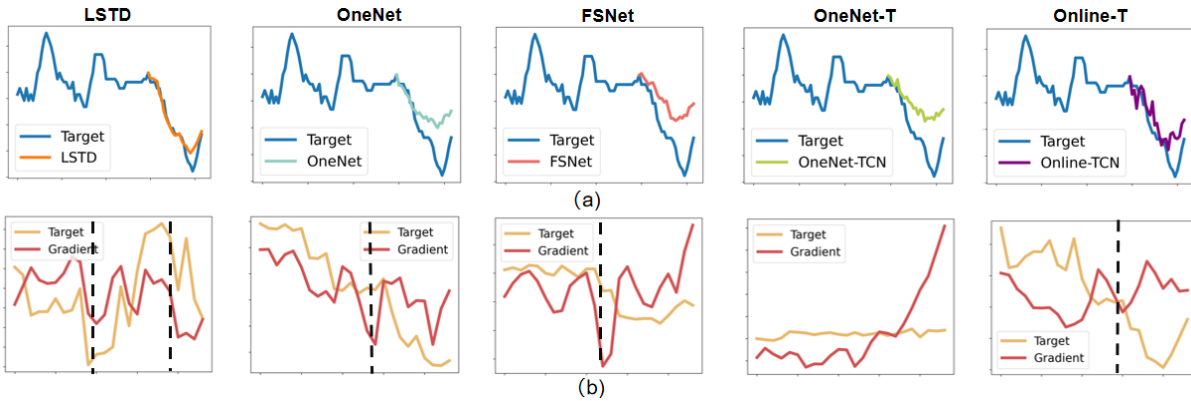


Figure 4: The figure (a) represents the visualization of the proposed LSTD and other baselines. The blue lines denote the ground-truth time series data and the lines with other colors denote the predicted results of different methods. The figure (b) shows the visualization of the LSTD method for detecting interventions. The yellow lines represent the real-time series data, and the red lines represent the gradient. Black dotted lines denote intervention occurs. (Best view in color)

tention of the information, implying that the retention benefits the preserving of the long-term effects and improves the forecasting performance. 3) Both long-term and short-term priors play an important role in forecasting, implying that these priors can capture temporal information.

## Summary

This paper presents a long/short-term state disentanglement model to address the challenges of online time-series forecasting in the presence of nonstationarity led by unknown interventions. Unlike existing methods, this model can theoretically identify both long-term and short-term latent variables, enhancing its relevance to real-world data. Technologically, the LSTD model employs the smooth constraint and sparse dependency constraint to enforce the disentanglement of long/short-term variables. In summary, this paper offers

valuable insights into enhancing online time-series forecasting via causal representation learning.

## Acknowledgments

This research was supported in part by National Science and Technology Major Project (2021ZD0111501), National Science Fund for Excellent Young Scholars (62122022) and Natural Science Foundation of China (U24A20233, 62206064, 62206061).

## References

Aljundi, R.; Belilovsky, E.; Tuytelaars, T.; Charlin, L.; Caccia, M.; Lin, M.; and Page-Caccia, L. 2019. Online continual learning with maximal interfered retrieval. *Conference and Workshop on Neural Information Processing Systems*, 32.

Aljundi, R.; Kelchtermans, K.; and Tuytelaars, T. 2019.

Task-free continual learning. In *IEEE Conference on Computer Vision and Pattern Recognition*, 11254–11263.

Anava, O.; Hazan, E.; Mannor, S.; and Shamir, O. 2013. Online learning for time series prediction. In *Conference on learning theory*, 172–184. Proceedings of Machine Learning Research.

Aydore, S.; Zhu, T.; and Foster, D. P. 2019. Dynamic local regret for non-convex online forecasting. *Conference and Workshop on Neural Information Processing Systems*, 32.

Bai, S.; Kolter, J. Z.; and Koltun, V. 2018. An empirical evaluation of generic convolutional and recurrent networks for sequence modeling. *arXiv preprint arXiv:1803.01271*.

Buzzega, P.; Boschini, M.; Porrello, A.; Abati, D.; and Calderara, S. 2020. Dark experience for general continual learning: a strong, simple baseline. *Conference and Workshop on Neural Information Processing Systems*, 33: 15920–15930.

Cai, Z.; Jiang, R.; Yang, X.; Wang, Z.; Guo, D.; Kobayashi, H.; Song, X.; and Shibasaki, R. 2023. Memda: forecasting urban time series with memory-based drift adaptation. *Conference on Information and Knowledge Management*, 2023.

Cao, J.; Li, Z.; and Li, J. 2019. Financial time series forecasting model based on CEEMDAN and LSTM. *Physica A: Statistical mechanics and its applications*, 519: 127–139.

Chaudhry, A.; Rohrbach, M.; Elhoseiny, M.; Ajanthan, T.; Dokania, P. K.; Torr, P. H.; and Ranzato, M. 2019. On tiny episodic memories in continual learning. *arXiv preprint arXiv:1902.10486*.

Clements, M. P.; Franses, P. H.; and Swanson, N. R. 2004. Forecasting economic and financial time-series with nonlinear models. *Int. J. Forecast.*, 20(2): 169–183.

Comon, P. 1994. Independent component analysis, a new concept? *Signal processing*, 36(3): 287–314.

Daunhawer, I.; Bizeul, A.; Palumbo, E.; Marx, A.; and Vogt, J. E. 2023. Identifiability results for multimodal contrastive learning. *International Conference on Learning Representations 2023*.

Graves, A.; and Graves, A. 2012. Long short-term memory. *Supervised sequence labelling with recurrent neural networks*, 37–45.

Gresele, L.; Rubenstein, P. K.; Mehrjou, A.; Locatello, F.; and Schölkopf, B. 2020. The incomplete rosetta stone problem: Identifiability results for multi-view nonlinear ica. In *UAI*, 217–227. Proceedings of Machine Learning Research.

Grossberg, S. 2013. Adaptive Resonance Theory: How a brain learns to consciously attend, learn, and recognize a changing world. *Neural networks*, 37: 1–47.

Gu, A.; Goel, K.; Gupta, A.; and Ré, C. 2022. On the parameterization and initialization of diagonal state space models. *Conference and Workshop on Neural Information Processing Systems*, 35: 35971–35983.

Gu, A.; Goel, K.; and Ré, C. 2021. Efficiently modeling long sequences with structured state spaces. *arXiv preprint arXiv:2111.00396*.

Gu, A.; Johnson, I.; Goel, K.; Saab, K.; Dao, T.; Rudra, A.; and Ré, C. 2021. Combining recurrent, convolutional, and continuous-time models with linear state space layers. *Conference and Workshop on Neural Information Processing Systems*, 34: 572–585.

Gultekin, S.; and Paisley, J. 2018. Online forecasting matrix factorization. *IEEE Transactions on Signal Processing*, 67(5): 1223–1236.

Guo, P.; Jin, P.; Li, Z.; Bai, L.; and Zhang, Y. 2024. Online Test-Time Adaptation of Spatial-Temporal Traffic Flow Forecasting. *arXiv preprint arXiv:2401.04148*.

Hälvä, H.; and Hyvärinen, A. 2020. Hidden markov nonlinear ica: Unsupervised learning from nonstationary time series. In *Conference on UAI*, 939–948. Proceedings of Machine Learning Research.

Hamilton, J. D. 2020. *Time series analysis*. Princeton university press.

Huang, Z.; Wang, H.; Zhao, J.; and Zheng, N. 2023. Latent processes identification from multi-view time series. *International Joint Conference on Artificial Intelligence-23*.

Hyvärinen, A. 2013. Independent component analysis: recent advances. *Philos. Trans. Royal Soc. A*, 371(1984): 20110534.

Hyvärinen, A.; Khemakhem, I.; and Monti, R. 2024. Identifiability of latent-variable and structural-equation models: from linear to nonlinear. *Ann Inst Stat Math*, 76(1): 1–33.

Hyvärinen, A.; and Morioka, H. 2016. Unsupervised feature extraction by time-contrastive learning and nonlinear ica. *Conference and Workshop on Neural Information Processing Systems*, 29.

Hyvärinen, A.; and Morioka, H. 2017. Nonlinear ICA of temporally dependent stationary sources. In *AISTATS*, 460–469. Proceedings of Machine Learning Research.

Hyvärinen, A.; and Pajunen, P. 1999. Nonlinear independent component analysis: Existence and uniqueness results. *Neural networks*, 12(3): 429–439.

Hyvärinen, A.; Sasaki, H.; and Turner, R. 2019. Nonlinear ICA using auxiliary variables and generalized contrastive learning. In *The 22nd International Conference on AISTATS*, 859–868. Proceedings of Machine Learning Research.

Khemakhem, I.; Kingma, D.; Monti, R.; and Hyvärinen, A. 2020a. Variational autoencoders and nonlinear ica: A unifying framework. In *International conference on AISTATS*, 2207–2217. Proceedings of Machine Learning Research.

Khemakhem, I.; Monti, R.; Kingma, D.; and Hyvärinen, A. 2020b. Ice-beem: Identifiable conditional energy-based deep models based on nonlinear ica. *Conference and Workshop on Neural Information Processing Systems*, 33: 12768–12778.

Kitaev, N.; Kaiser, Ł.; and Levskaya, A. 2020. Reformer: The efficient transformer. *arXiv preprint arXiv:2001.04451*.

Kong, L.; Huang, B.; Xie, F.; Xing, E.; Chi, Y.; and Zhang, K. 2023a. Identification of nonlinear latent hierarchical models. *Conference and Workshop on Neural Information Processing Systems*, 36: 2010–2032.

Kong, L.; Ma, M. Q.; Chen, G.; Xing, E. P.; Chi, Y.; Morency, L.-P.; and Zhang, K. 2023b. Understanding masked autoencoders via hierarchical latent variable models. In *IEEE Conference on Computer Vision and Pattern Recognition*, 7918–7928.

Kong, L.; Xie, S.; Yao, W.; Zheng, Y.; Chen, G.; Stojanov, P.; Akinwande, V.; and Zhang, K. 2022. Partial disentanglement for domain adaptation. In *International Conference on Machine Learning*, 11455–11472. Proceedings of Machine Learning Research.

Lachapelle, S.; Deleu, T.; Mahajan, D.; Mitliagkas, I.; Bengio, Y.; Lacoste-Julien, S.; and Bertrand, Q. 2023. Synergies between disentanglement and sparsity: Generalization and identifiability in multi-task learning. In *International Conference on Machine Learning*, 18171–18206. Proceedings of Machine Learning Research.

Lachapelle, S.; and Lacoste-Julien, S. 2022. Partial disentanglement via mechanism sparsity. *CRL* 2022.

Lai, G.; Chang, W.-C.; Yang, Y.; and Liu, H. 2018. Modeling long-and short-term temporal patterns with deep neural networks. In *The 41st international ACM SIGIR conference on research & development in information retrieval*, 95–104.

Lee, T.-W.; and Lee, T.-W. 1998. *Independent component analysis*. Springer.

Li, Z.; Cai, R.; Chen, G.; Sun, B.; Hao, Z.; and Zhang, K. 2024a. Subspace identification for multi-source domain adaptation. *Conference and Workshop on Neural Information Processing Systems*, 36.

Li, Z.; Cai, R.; Yang, Z.; Huang, H.; Chen, G.; Shen, Y.; Chen, Z.; Song, X.; Hao, Z.; and Zhang, K. 2024b. When and How: Learning Identifiable Latent States for Nonstationary Time Series Forecasting. *arXiv preprint arXiv:2402.12767*.

Li, Z.; Shen, Y.; Zheng, K.; Cai, R.; Song, X.; Gong, M.; Zhu, Z.; Chen, G.; and Zhang, K. 2024c. On the identification of temporally causal representation with instantaneous dependence. *arXiv preprint arXiv:2405.15325*.

Li, Z.; Xu, Z.; Cai, R.; Yang, Z.; Yan, Y.; Hao, Z.; Chen, G.; and Zhang, K. 2023. Identifying Semantic Component for Robust Molecular Property Prediction. *arXiv preprint arXiv:2311.04837*.

Lin, L.-J. 1992. Self-improving reactive agents based on reinforcement learning, planning and teaching. *Machine learning*, 8: 293–321.

Lippe, P.; Magliacane, S.; Löwe, S.; Asano, Y. M.; Cohen, T.; and Gavves, S. 2022. Citris: Causal identifiability from temporal intervened sequences. In *International Conference on Machine Learning*, 13557–13603. Proceedings of Machine Learning Research.

Lippi, M.; Bertini, M.; and Frasconi, P. 2013. Short-term traffic flow forecasting: An experimental comparison of time-series analysis and supervised learning. *IEEE trans Intell Transp Syst*, 14(2): 871–882.

Liu, C.; Hoi, S. C.; Zhao, P.; and Sun, J. 2016. Online arima algorithms for time series prediction. In *Association for the Advancement of Artificial Intelligence*, volume 30.

Liu, S.; Yu, H.; Liao, C.; Li, J.; Lin, W.; Liu, A. X.; and Dustdar, S. 2021. Pyraformer: Low-complexity pyramidal attention for long-range time series modeling and forecasting. In *International conference on learning representations*.

Liu, Y.; Alahi, A.; Russell, C.; Horn, M.; Zietlow, D.; Schölkopf, B.; and Locatello, F. 2023a. Causal triplet: An open challenge for intervention-centric causal representation learning. In *Conference on CLeaR*, 553–573. Proceedings of Machine Learning Research.

Liu, Y.; Hu, T.; Zhang, H.; Wu, H.; Wang, S.; Ma, L.; and Long, M. 2023b. itransformer: Inverted transformers are effective for time series forecasting. *International Conference on Learning Representations 2024*.

Lopez-Paz, D.; and Ranzato, M. 2017. Gradient episodic memory for continual learning. *Conference and Workshop on Neural Information Processing Systems*, 30.

Luan, Z.; Wang, H.; Zhang, L.; Liang, S.; and Han, W. 2024. Online Prediction for Streaming Tensor Time Series. *arXiv preprint arXiv:2403.18320*.

Mansouri, A.; Hartford, J.; Zhang, Y.; and Bengio, Y. 2023. Object-centric architectures enable efficient causal representation learning. *International Conference on Learning Representations 2024*.

Mejri, M.; Amarnath, C.; and Chatterjee, A. 2024. A Novel Hyperdimensional Computing Framework for Online Time Series Forecasting on the Edge. *arXiv preprint arXiv:2402.01999*.

Nie, Y.; Nguyen, N. H.; Sinhong, P.; and Kalagnanam, J. 2022. A time series is worth 64 words: Long-term forecasting with transformers. *International Conference on Learning Representations 2023*.

Oreshkin, B. N.; Carpow, D.; Chapados, N.; and Bengio, Y. 2019. N-BEATS: Neural basis expansion analysis for interpretable time series forecasting. *arXiv preprint arXiv:1905.10437*.

Pan, Z.; Jiang, Y.; Song, D.; Garg, S.; Rasul, K.; Schneider, A.; and Nevmyvaka, Y. 2024. Structural Knowledge Informed Continual Multivariate Time Series Forecasting. *arXiv preprint arXiv:2402.12722*.

Pham, Q.; Liu, C.; Sahoo, D.; and Hoi, S. C. 2022. Learning fast and slow for online time series forecasting. *International Conference on Learning Representations 2023*.

Rajendran, G.; Buchholz, S.; Aragam, B.; Schölkopf, B.; and Ravikumar, P. 2024. Learning interpretable concepts: Unifying causal representation learning and foundation models. *Conference and Workshop on Neural Information Processing Systems 2024*.

Salinas, D.; Flunkert, V.; Gasthaus, J.; and Januschowski, T. 2020. DeepAR: Probabilistic forecasting with autoregressive recurrent networks. *Int. J. Forecast.*, 36(3): 1181–1191.

Schölkopf, B.; Locatello, F.; Bauer, S.; Ke, N. R.; Kalchbrenner, N.; Goyal, A.; and Bengio, Y. 2021. Toward causal representation learning. *Proceedings of the IEEE*, 109(5): 612–634.

Song, X.; Yao, W.; Fan, Y.; Dong, X.; Chen, G.; Niebles, J. C.; Xing, E.; and Zhang, K. 2024. Temporally disentangled representation learning under unknown nonstationarity. *Conference and Workshop on Neural Information Processing Systems*, 36.

Wang, H.; Peng, J.; Huang, F.; Wang, J.; Chen, J.; and Xiao, Y. ???? Micn: Multi-scale local and global context modeling for long-term series forecasting. In *The eleventh international conference on learning representations*.

Wang, R.; Dong, Y.; Arik, S. Ö.; and Yu, R. 2022. Koopman neural forecaster for time series with temporal distribution shifts. *International Conference on Learning Representations 2023*.

Wen, Q.; Chen, W.; Sun, L.; Zhang, Z.; Wang, L.; Jin, R.; Tan, T.; et al. 2024. Onenet: Enhancing time series forecasting models under concept drift by online ensembling. *Conference and Workshop on Neural Information Processing Systems*, 36.

Wendong, L.; Kekić, A.; von Kügelgen, J.; Buchholz, S.; Besserve, M.; Gresele, L.; and Schölkopf, B. 2024. Causal component analysis. *Conference and Workshop on Neural Information Processing Systems*, 36.

Wu, H.; Hu, T.; Liu, Y.; Zhou, H.; Wang, J.; and Long, M. 2022. Timesnet: Temporal 2d-variation modeling for general time series analysis. *arXiv preprint arXiv:2210.02186*.

Wu, H.; Xu, J.; Wang, J.; and Long, M. 2021. Autoformer: Decomposition transformers with auto-correlation for long-term series forecasting. *Conference and Workshop on Neural Information Processing Systems*, 34: 22419–22430.

Xie, S.; Kong, L.; Gong, M.; and Zhang, K. 2023. Multi-domain image generation and translation with identifiability guarantees. In *The Eleventh International Conference on Learning Representations*.

Yan, H.; Kong, L.; Gui, L.; Chi, Y.; Xing, E.; He, Y.; and Zhang, K. 2024. Counterfactual generation with identifiability guarantees. *Conference and Workshop on Neural Information Processing Systems*, 36.

Yao, D.; Xu, D.; Lachapelle, S.; Magliacane, S.; Taslakian, P.; Martius, G.; von Kügelgen, J.; and Locatello, F. 2023. Multi-view causal representation learning with partial observability. *International Conference on Learning Representations 2024*.

Yao, W.; Chen, G.; and Zhang, K. 2022. Temporally disentangled representation learning. *Conference and Workshop on Neural Information Processing Systems*, 35: 26492–26503.

Yao, W.; Sun, Y.; Ho, A.; Sun, C.; and Zhang, K. 2021. Learning temporally causal latent processes from general temporal data. *International Conference on Learning Representations 2022*.

Zeng, A.; Chen, M.; Zhang, L.; and Xu, Q. 2023. Are transformers effective for time series forecasting? In *Association for the Advancement of Artificial Intelligence*, volume 37, 11121–11128.

Zhang, K.; and Chan, L. 2007. Kernel-based nonlinear independent component analysis. In *International Conference on Independent Component Analysis and Signal Separation*, 301–308. Springer.

Zhang, K.; Xie, S.; Ng, I.; and Zheng, Y. 2024a. Causal representation learning from multiple distributions: A general setting. *International Conference on Machine Learning 2024*.

Zhang, T.; Zhang, Y.; Cao, W.; Bian, J.; Yi, X.; Zheng, S.; and Li, J. 2022. Less is more: Fast multivariate time series forecasting with light sampling-oriented mlp structures. *arXiv preprint arXiv:2207.01186*.

Zhang, Y.; Chen, W.; Zhu, Z.; Qin, D.; Sun, L.; Wang, X.; Wen, Q.; Zhang, Z.; Wang, L.; and Jin, R. 2024b. Addressing Concept Shift in Online Time Series Forecasting: Detect-then-Adapt. *arXiv preprint arXiv:2403.14949*.

Zheng, Y.; Ng, I.; and Zhang, K. 2022. On the identifiability of nonlinear ICA: Sparsity and beyond. *Conference and Workshop on Neural Information Processing Systems*, 35: 16411–16422.

Zhou, H.; Zhang, S.; Peng, J.; Zhang, S.; Li, J.; Xiong, H.; and Zhang, W. 2021. Informer: Beyond efficient transformer for long sequence time-series forecasting. In *Association for the Advancement of Artificial Intelligence*, volume 35, 11106–11115.

Zinkevich, M. 2003. Online convex programming and generalized infinitesimal gradient ascent. In *International Conference on Machine Learning*, 928–936.

## A. Related Works

### Time Series Forecasting

Recently, various research studies focused on time series forecasting problems, and deep learning-based methods have been very successful in this field. More precisely, the deep learning-based methods can be divided into several classes. First, the model based on RNN utilizes a recursive structure with memory to construct hidden layer transitions over time points .(Graves and Graves 2012; Lai et al. 2018; Salinas et al. 2020). Second, TCN (Bai, Kolter, and Koltun 2018; Wang et al.; Wu et al. 2022) based approach to modeling hierarchical temporal patterns and extracting features using a shared convolutional kernel. Besides, there are simple but very effective methods as well, such as based on MLP (Oreshkin et al. 2019; Zeng et al. 2023; Zhang et al. 2022; Li et al. 2024b) and on states-base-model (Gu et al. 2022, 2021; Gu, Goel, and Ré 2021). Above these methods, the Transformer methods are especially outstanding and get the great process on the time series forecasting task (Kitaev, Kaiser, and Levskaya 2020; Liu et al. 2021; Wu et al. 2021; Zhou et al. 2021). However, these existing methods are based on offline data processing, contrary to the mainstream ONLINE training methods of the significant data era. Since the above methods are unsuitable for direct application to online problems, a model that can be trained on online data and perform well is needed.

### Online Time Series Forecasting

Due to the rapid increase in train data and the requirement for model updates online, online time series forecasting has become more popular than offline ones(Anava et al. 2013; Liu et al. 2016; Gultekin and Paisley 2018; Aydore, Zhu, and Foster 2019). (Pan et al. 2024) employs structural consistency regularization to capture a range of scenarios, using a representation-matching memory replay scheme to retain temporal dynamics and dependencies. (Luan et al. 2024) applies tensor factorization for streaming tensor time series prediction, updating the predictor in a low-complexity online manner to adapt to evolving data. (Mejri, Amarnath, and Chatterjee 2024) addresses online nonlinear time-series forecasting by mapping low-dimensional series to high-dimensional spaces for linear hyperdimensional prediction, adapting to temporal distribution shifts. Online time series forecasting is a widely used technique in the real world due to the continuity of the data and the frequent drift of concepts. In this approach, the learning process occurs over a series of rounds. The model receives a look-back window, predicts the forecasting window, and then displays the valid values to improve the model's performance in the next round. Recently, a brunch of online time series forecasting work got excellent results, including considering gradient updates to optimize fast new as well as retained information (Pham et al. 2022) and models that consider both temporal and feature dimensions (Wen et al. 2024). Nevertheless, the fast adaptation and information retention of the models mentioned above are simultaneous. It needs to decouple the long and short term, which can lead to confounding results and suboptimal predictions. To solve this problem, the LSTD decouples the data first to isolate the long and short-term effects on the prediction, with the long-term effects being used to preserve the characteristics of the historical data and the short-term effects being used to quickly adapt to changes in the data for better online prediction.

### Continual Learning

Continual learning is a novel topic and aims to set up intelligent agency by learning the sequence of tasks to perform with restricted access to experience (Lopez-Paz and Ranzato 2017). A continual learning model must balance the knowledge of the current task and the prompt of the future learning process, as known in the stability-plasticity dilemma (Lin 1992; Grossberg 2013). Due to their connection to how humans learn, several neuroscience frameworks have prompted the development of various continual learning algorithms. The continual learning model corresponds to the requirement of online time series forecasting. The constant learning can enable real-time updates upon receiving the new data to adapt the data dynamics better, improving the model accuracy. The proposed LSTD incorporates continual learning into an online time series forecasting model, which mitigates the stability-plasticity problem by decoupling the long and short-term effects, retaining the knowledge of previous tasks through the long-term effects, and facilitating the learning of future tasks through the short-term effects.

### Causal Representation Learning

To recover the latent variable with identification guarantees(Yao et al. 2023; Schölkopf et al. 2021; Liu et al. 2023a; Greselle et al. 2020), independent component analysis (ICA) has been used in a number of studies to determine the causal representation (Rajendran et al. 2024; Mansouri et al. 2023; Wendong et al. 2024; Li et al. 2024c). Conventional approaches presuppose a linear mixing function for latent and observable variables. (Comon 1994; Hyvärinen 2013; Lee and Lee 1998; Zhang and Chan 2007). However, determining the linear mixing function is a difficult problem in real-world situations. For the identifiability, many assumptions are made throughout the nonlinear ICA process, including the sparse generation process and the usage of auxiliary variables(Zheng, Ng, and Zhang 2022; Hyvärinen and Pajunen 1999; Hyvärinen, Khemakhem, and Monti 2024; Khemakhem et al. 2020b; Li et al. 2023).

Specifically, Aapo et al.'s study confirms identifiability first. The exponential family is assumed to consist of latent sources in Ref. (Khemakhem et al. 2020a; Hyvarinen and Morioka 2016, 2017; Hyvarinen, Sasaki, and Turner 2019), where auxiliary variables such as domain indexes, time indexes, and class labels are added. Furthermore, Zhang et al.'s study (Kong et al. 2022; Xie et al. 2023; Kong et al. 2023a; Yan et al. 2024) demonstrates that the exponential family assumption is not necessary to accomplish component-wise identification for nonlinear ICA.

Sparsity assumptions were used in several study endeavors to attain identifiability without supervised signals (Zheng, Ng, and Zhang 2022; Hyvärinen and Pajunen 1999; Hyvärinen, Khemakhem, and Monti 2024; Khemakhem et al. 2020b; Li et al. 2023). For example, Lachapelle et al. (Lachapelle et al. 2023; Lachapelle and Lacoste-Julien 2022) presented mechanism sparsity regularization as an inductive bias to find causative latent components. Zhang et al. selected the latent variable sparse structures in Ref. (Zhang et al. 2024a) to achieve identifiability under distribution shift. Furthermore, nonlinear ICA was utilized in Ref. (Hyvärinen and Morioka 2016; Yan et al. 2024; Huang et al. 2023; Hälvä and Hyvärinen 2020; Lippe et al. 2022) to get the identifiability of time series data. Premise and capitalization of variance variations across data segments based on separate sources were utilized in the study by Aapo et al. (Hyvärinen and Morioka 2016) to detect nonstationary time series data identifiability. Conversely, the latent variables in stationary time series data are found via permutation-based contrastive learning. Independent noise and variability history information features have been used more recently in TDRL (Yao, Chen, and Zhang 2022) and LEAP (Yao et al. 2021).

Simultaneously, latent variables were discovered by Song et al. (Song et al. 2024) without the need to observe the domain variables. Imant et al. (Daunhawer et al. 2023) described multimodal comparative learning as having identifiability in terms of modality. Yao et al. (Yao et al. 2023) postulated that multi-perspective causal representations can still be identified when there are incomplete observations. This paper uses multi-modality time series data and leverages historical variability information and multi-modality data fairness to demonstrate identifiability.

## B. Proof

### Identification

In this section, we provide the definition of different types of identification.

**Subspace Identification** For each ground-truth changing latent variables  $z_{t,i}$ , the subspace identification means that there exists  $\hat{z}_t$  and an invertible function  $z_{t,i} = h_i(\hat{z}_t)$ , such that  $z_{t,i} = h_i(\hat{z}_t)$ .

### Identification Guarantees

#### Subspace of Identification Long/Short-term Latent Variables

**Theorem 2. (Subspace of Identification Long/Short-term Latent Variables  $\mathbf{z}_t^s$  and  $\mathbf{z}_t^d$ .)** We follow the data generation process in Figure 1 (c) and Equation (1)-(3) and make the following assumptions:

- A1 (Smooth, Positive and Conditional independent Density:) (Yao, Chen, and Zhang 2022; Yao et al. 2021) The probability density function of latent variables is smooth and positive, i.e.,  $p(\mathbf{z}_{t-\tau+1:t} | \mathbf{z}_{t-\tau}) > 0$  over  $\mathbf{z}_{t-\tau}$  and  $\mathbf{z}_{t-\tau+1:t}$ . Conditioned on  $\mathbf{z}_{t-\tau}$  each  $z_i$  is independent of any other  $z_j$  for  $i, j \in 1, \dots, n, i \neq j$ , i.e.,  $\log p(\mathbf{z}_{t-\tau+1:t} | \mathbf{z}_{t-\tau}) = \sum_{k=1}^{n_s} \log p(z_{t-\tau+1:t,k} | \mathbf{z}_{t-\tau})$
- A2 (non-singular Jacobian:) (Kong et al. 2023b) Each generating function  $g$  has non-singular Jacobian matrices almost anywhere and  $g$  is invertible.
- A3 (Linear Independence:) (Yao, Chen, and Zhang 2022) For any  $\mathbf{z}^d \in Z_{t-\tau+1:t}^d \subseteq R^{n_d}$ ,  $\bar{v}_{t-\tau,1}, \dots, \bar{v}_{t-\tau,n_d}$  as  $n_d$  vector functions in  $z_{t-\tau,1}^d, \dots, z_{t-\tau,l}^d, \dots, z_{t-\tau,n_d}^d$  are linear independent, where  $\bar{v}_{t-\tau,l}$  are formalized as follows:

$$\bar{v}_{t-\tau,l} = \frac{\partial^2 \log p(\mathbf{z}_{t-\tau+1:t}^d | \mathbf{z}_{t-\tau}^d)}{\partial z_{t-\tau+1:t,k}^d \partial z_{t-\tau,l}^d} \quad (B.17)$$

Suppose that we learn  $(\hat{g}, \hat{f}_i^s, \hat{f}_i^d)$  to achieve Equation (1)-(3) with the minimal number of transition edge among short term latent variables  $\mathbf{z}_1^d, \dots, \mathbf{z}_t^d, \dots$ , then the long-term and short-term latent variables are block-wise identifiable.

*Proof.* First, we can view the data generation process as two parts. Separating the time series is helpful for us to identify, as interventions occur in the time series process, The specific process is as follows:

$$\mathbf{x}_{t-\tau-1:t} = g(\mathbf{z}_{t-\tau-1:t}^d, \mathbf{z}_{t-\tau-1:t}^s) \quad (B.18)$$

$$\mathbf{x}_{t-\tau-1} = g_1(\mathbf{z}_{t-\tau-1}^d, \mathbf{z}_{t-\tau-1:t}^s) \quad (B.19)$$

$$\mathbf{x}_{t-\tau+1:t} = g_2(\mathbf{z}_{t-\tau+1:t}^d, \mathbf{z}_{t-\tau-1:t}^s), \quad (B.20)$$

where time lag is  $\tau + 1$ ,  $\mathbf{z}_{t-\tau-1:t}^s \in \mathbf{z}^s \subset R^{n_s}$ ,  $\mathbf{z}_{t-\tau-1}^d \in \mathbf{z}_1^d \subset R^{n_d}$ ,  $\mathbf{z}_{t-\tau+1:t}^d \in \mathbf{z}_2^d \subset R^{n_d^2}$ . This involves an intervention at time  $t - \tau - 1$ , resulting in an interrupted edge between short-term latent  $\mathbf{z}_{t-\tau-1}^d$  and  $\mathbf{z}_{t-\tau}^d$ . Whereas  $\mathbf{z}_{t-\tau-1:t}^s$  represents a long-term latent, it is not subject to intervention interruption, and therefore is shared by the two components. Of note, the first  $z^d$  after the break is unrecognizable because it lacks supervisory signals; hence, we omit  $\mathbf{z}_{t-\tau}^d$  here. And We will take  $\mathbf{z}_{t-\tau}^d$  as the supervision signal for the subsequent consecutive points. Besides, Both  $g_1$  and  $g_2$  are smooth and have non-singular Jacobian matrices almost anywhere. Let's denote  $\hat{g}_1 : Z \rightarrow V_1 \in \mathbf{x}_{t-\tau-1}$  and  $\hat{g}_2 : Z \rightarrow V_2 \in \mathbf{x}_{t-\tau+1:t}$ , the generating process of the true model  $(g_1, g_2)$  and match the joint distribution  $p_{v_1, v_2}$

For  $(v_1, v_2) \sim p_{v_1, v_2}$  because of the matched joint distribution, we have the following relations between the true variables  $(\mathbf{z}_{t-\tau-1:t}^s, \mathbf{z}_{t-\tau-1}^d, \mathbf{z}_{t-\tau+1:t}^d)$  and the estimated ones  $(\hat{\mathbf{z}}_{t-\tau-1:t}^s, \hat{\mathbf{z}}_{t-\tau-1}^d, \hat{\mathbf{z}}_{t-\tau+1:t}^d)$ :

$$\mathbf{x}_{t-\tau-1} = g_1(\mathbf{z}_{t-\tau-1:t}^s, \mathbf{z}_{t-\tau-1}^d) = \hat{g}_1(\hat{\mathbf{z}}_{t-\tau-1:t}^s, \hat{\mathbf{z}}_{t-\tau-1}^d) \quad (\text{B.21})$$

$$\mathbf{x}_{t-\tau+1:t} = g_2(\mathbf{z}_{t-\tau-1:t}^s, \mathbf{z}_{t-\tau+1:t}^d) = \hat{g}_2(\hat{\mathbf{z}}_{t-\tau-1:t}^s, \hat{\mathbf{z}}_{t-\tau+1:t}^d) \quad (\text{B.22})$$

$$\begin{aligned} (\hat{\mathbf{z}}_{t-\tau-1:t}^s, \hat{\mathbf{z}}_{t-\tau-1}^d, \hat{\mathbf{z}}_{t-\tau+1:t}^d) &= \hat{g}^{-1}(\mathbf{x}_{t-\tau-1}, \mathbf{x}_{t-\tau+1:t}) = \hat{g}^{-1}(g(\mathbf{z}_{t-\tau-1:t}^s, \mathbf{z}_{t-\tau-1}^d, \mathbf{z}_{t-\tau+1:t}^d)) \\ &:= h(\mathbf{z}_{t-\tau-1:t}^s, \mathbf{z}_{t-\tau-1}^d, \mathbf{z}_{t-\tau+1:t}^d), \end{aligned} \quad (\text{B.23})$$

where  $\hat{g}_1, \hat{g}_2$  are the estimated invertible generating function and we define the smooth and invertible function  $h := \hat{g}^{-1} \circ g$  that transforms the true variables  $(\mathbf{z}_{t-\tau-1:t}^s, \mathbf{z}_{t-\tau-1}^d, \mathbf{z}_{t-\tau+1:t}^d)$  to estimates  $(\hat{\mathbf{z}}_{t-\tau-1:t}^s, \hat{\mathbf{z}}_{t-\tau-1}^d, \hat{\mathbf{z}}_{t-\tau+1:t}^d)$ . By combining Equation (B.23) and (B.21), we have :

$$g_1(\mathbf{z}_{t-\tau-1:t}^s, \mathbf{z}_{t-\tau-1}^d) = \hat{g}_1(h_{\mathbf{z}_{t-\tau-1:t}^s, \mathbf{z}_{t-\tau-1}^d}(\mathbf{z}_{t-\tau-1:t}^s, \mathbf{z}_{t-\tau-1}^d, \mathbf{z}_{t-\tau+1:t}^d)), \quad (\text{B.24})$$

For  $i \in \{1, \dots, n_d^1\}$  and  $j \in \{1, \dots, n_d^2\}$  taking partial derivative of the  $j$ -th dimension of both sides of Equation (B.24) w.r.t.  $z_{t-\tau+1:t,j}^d$  and have:

$$0 = \frac{\partial g_{1,i}(\mathbf{z}_{t-\tau-1:t}^s, \mathbf{z}_{t-\tau-1}^d)}{\partial z_{t-\tau+1:t,j}^d} = \frac{\partial \hat{g}_{1,i}(h_{\mathbf{z}_{t-\tau-1:t}^s, \mathbf{z}_{t-\tau-1}^d}(\mathbf{z}_{t-\tau-1:t}^s, \mathbf{z}_{t-\tau-1}^d))}{\partial z_{t-\tau+1:t,j}^d}, \quad (\text{B.25})$$

The aforementioned equation equals 0 because there is no  $z_{t-\tau+1:t,j}^d$  in the left-hand side of the equation. By expanding the derivative on the right-hand side, we further have:

$$\sum_{k \in \{1, \dots, n_s + n_d^1\}} \frac{\partial \hat{g}_{1,i}}{\partial h_{(\mathbf{z}_{t-\tau-1:t}^s, \mathbf{z}_{t-\tau-1}^d), k}} \cdot \frac{\partial h_{(\mathbf{z}_{t-\tau-1:t}^s, \mathbf{z}_{t-\tau-1}^d), k}}{\partial z_{t-\tau+1:t,j}^d}(\mathbf{z}_{t-\tau-1:t}^s, \mathbf{z}_{t-\tau-1}^d, \mathbf{z}_{t-\tau+1:t}^d) = 0, \quad (\text{B.26})$$

Since  $\hat{g}_1$  is invertible, the determinant of  $J_{\hat{g}_1}$  does not equal to 0, meaning that for  $n_s + n_d^1$  different values of  $\hat{g}_{1,i}$ , each vector  $[\frac{\partial \hat{g}_{1,i}}{\partial h_{(\mathbf{z}_{t-\tau-1:t}^s, \mathbf{z}_{t-\tau-1}^d), 1}}, \dots, \frac{\partial \hat{g}_{1,i}}{\partial h_{(\mathbf{z}_{t-\tau-1:t}^s, \mathbf{z}_{t-\tau-1}^d), n_s + n_d^1}}]$  are linearly independent. Therefore, the  $(n_s + n_d^1) \times (n_s + n_d^1)$  linear system is invertible and has the unique solution as follows:

$$\frac{\partial h_{(\mathbf{z}_{t-\tau-1:t}^s, \mathbf{z}_{t-\tau-1}^d), k}}{\partial z_{t-\tau+1:t,j}^d}(\mathbf{z}_{t-\tau-1:t}^s, \mathbf{z}_{t-\tau-1}^d, \mathbf{z}_{t-\tau+1:t}^d) = 0, \quad (\text{B.27})$$

According to Equation (B.27) for any  $k \in \{1, \dots, n_s + n_d^1\}$  and  $j \in \{1, \dots, n_d^2\}$ ,  $h_{(\mathbf{z}_{t-\tau-1:t}^s, \mathbf{z}_{t-\tau-1}^d), k}$  does not depend on  $\mathbf{z}_{t-\tau+1:t}^d$ . In other word,  $\{\hat{\mathbf{z}}_{t-\tau-1:t}^s, \hat{\mathbf{z}}_{t-\tau-1}^d\}$  does not depend on  $\hat{\mathbf{z}}_{t-\tau+1:t}^d$ . Applying the same reasoning to  $h_{(\mathbf{z}_{t-\tau-1:t}^s, \mathbf{z}_{t-\tau-1}^d), k}$ , we can obtain that  $h_{(\mathbf{z}_{t-\tau-1:t}^s, \mathbf{z}_{t-\tau-1}^d), k}$ , i.e.  $(\hat{\mathbf{z}}_{t-\tau-1:t}^s, \hat{\mathbf{z}}_{t-\tau-1}^d)$  does not depend on  $\mathbf{z}_{t-\tau-1}^d$ . Thus, for  $(\hat{\mathbf{z}}_{t-\tau-1:t}^s, \hat{\mathbf{z}}_{t-\tau-1}^d, \hat{\mathbf{z}}_{t-\tau+1:t}^d)$  we can observe that  $\hat{\mathbf{z}}_{t-\tau-1:t}^s$  does not depend on  $\mathbf{z}_{t-\tau+1:t}^d$  and  $\mathbf{z}_{t-\tau-1}^d$ , that is,  $\hat{\mathbf{z}}_{t-\tau-1:t}^s = h_{\mathbf{z}_{t-\tau-1:t}^s}(\mathbf{z}_{t-\tau-1:t}^s, \mathbf{z}_{t-\tau-1:t}^d)$  are subspace identifiable.

Since the matched marginal distribution of  $p(\mathbf{z}_{t-\tau+1:t} | \mathbf{x}_{t-\tau})$ , we have:

$$p(\hat{\mathbf{x}}_{t-\tau+1:t} | \mathbf{x}_{t-\tau}) = p(\mathbf{x}_{t-\tau+1:t} | \mathbf{x}_{t-\tau}) \iff p(\hat{g}(\hat{\mathbf{z}}_{t-\tau+1:t}) | \mathbf{x}_{t-\tau}) = p(g(\mathbf{z}_{t-\tau+1:t}) | \mathbf{x}_{t-\tau}), \quad (\text{B.28})$$

where  $\mathbf{z}_{t-\tau+1:t} = \{\mathbf{z}_{t-\tau+1:t}^s, \mathbf{z}_{t-\tau+1:t}^d\}$  and  $\hat{\mathbf{z}}_{t-\tau+1:t} = \{\hat{\mathbf{z}}_{t-\tau+1:t}^s, \hat{\mathbf{z}}_{t-\tau+1:t}^d\}$ . Sequentially, by using the change of variables formula, we can further obtain Equation (B.29)

$$\begin{aligned} p(\hat{g}(\hat{\mathbf{z}}_{t-\tau+1:t}) | \mathbf{x}_{t-\tau}) &= p(g(\mathbf{z}_{t-\tau+1:t}) | \mathbf{x}_{t-\tau}) \iff p(g^{-1} \circ \hat{g}(\hat{\mathbf{z}}_{t-\tau+1:t}) | \mathbf{x}_{t-\tau}) | \mathbf{J}_{g^{-1}} | = p(\mathbf{z}_{t-\tau+1:t} | \mathbf{x}_{t-\tau}) | \mathbf{J}_{g^{-1}} | \\ &\iff p(h(\hat{\mathbf{z}}_{t-\tau+1:t}) | \mathbf{x}_{t-\tau}) = p(\mathbf{z}_{t-\tau+1:t} | \mathbf{x}_{t-\tau}) \\ &\iff p(h(\hat{\mathbf{z}}_{t-\tau+1:t}) | \hat{\mathbf{z}}_{t-\tau}) = p(\mathbf{z}_{t-\tau+1:t} | \mathbf{z}_{t-\tau}), \end{aligned} \quad (\text{B.29})$$

where  $h := g^{-1} \circ \hat{g}_1$  is the transformation between the ground-true and the estimated latent variables.  $\mathbf{J}_{g^{-1}}$  denotes the absolute value of Jacobian matrix determinant of  $g^{-1}$ . Since we assume that  $g$  and  $\hat{g}$  are invertible,  $|\mathbf{J}_{g^{-1}}| \neq 0$  and  $h$  is also invertible.

According to the A1 (conditional independent assumption), we can have Equation (B.30)

$$\begin{aligned} p(\mathbf{z}_{t-\tau+1:t} | \mathbf{z}_{t-\tau}) &= \prod_{i=1}^n p(z_{t-\tau+1:t,i} | \mathbf{z}_{t-\tau}); \\ p(\hat{\mathbf{z}}_{t-\tau+1:t} | \hat{\mathbf{z}}_{t-\tau}) &= \prod_{i=1}^n p(\hat{z}_{t-\tau+1:t,i} | \hat{\mathbf{z}}_{t-\tau}). \end{aligned} \quad (\text{B.30})$$

For convenience, we take logarithm on both sides of Equation (B.30) and have:

$$\begin{aligned}\log p(\mathbf{z}_{t-\tau+1:t} | \mathbf{z}_{t-\tau}) &= \sum_{i=1}^n \log p(z_{t-\tau+1:t,i} | \mathbf{z}_{t-\tau}); \\ \log p(\hat{\mathbf{z}}_{t-\tau+1:t} | \hat{\mathbf{z}}_{t-\tau}) &= \sum_{i=1}^n \log p(\hat{z}_{t-\tau+1:t,i} | \hat{\mathbf{z}}_{t-\tau}).\end{aligned}\tag{B.31}$$

By combining Equation (B.31) and Equation (B.29), we have:

$$\begin{aligned}p(h(\hat{\mathbf{z}}_{t-\tau+1:t}) | \hat{\mathbf{z}}_{t-\tau}) &= p(\mathbf{z}_{t-\tau+1:t} | \mathbf{z}_{t-\tau}) \\ \iff p(\hat{\mathbf{z}}_{t-\tau+1:t} | \hat{\mathbf{z}}_{t-\tau}) |\mathbf{J}_{h^{-1}}| &= p(\mathbf{z}_{t-\tau+1:t} | \mathbf{z}_{t-\tau}) \\ \iff \log p(\hat{\mathbf{z}}_{t-\tau+1:t} | \hat{\mathbf{z}}_{t-\tau}) &= \sum_{k=1}^n \log p(z_{t-\tau+1:t,k} | \mathbf{z}_{t-\tau}) - \log |\mathbf{J}_{h^{-1}}|,\end{aligned}\tag{B.32}$$

where  $\mathbf{J}_{h^{-1}}$  are the Jacobian matrix of  $h^{-1}$ . Sequentially, we take the first-order derivative with  $\hat{z}_{t-\tau+1:t,i}$ , where  $i \in \{1, \dots, n_s\}$  and have:

$$\begin{aligned}\frac{\partial \log p(\hat{z}_{t-\tau+1:t} | \mathbf{z}_{t-\tau}^d)}{\partial \hat{z}_{t-\tau+1:t,i}^s} &= \sum_{k=1}^{n_s} \frac{\partial \log p(z_{t-\tau+1:t,k}^s | \mathbf{z}_{t-\tau}^d)}{\partial z_{t-\tau+1:t,k}^s} \cdot \frac{\partial z_{t-\tau+1:t,k}^s}{\partial \hat{z}_{t-\tau+1:t,i}^s} \\ &+ \sum_{k=n_s+1}^n \frac{\partial \log p(z_{t-\tau+1:t,k}^d | \mathbf{z}_{t-\tau}^d)}{\partial z_{t-\tau+1:t,k}^d} \cdot \frac{\partial z_{t-\tau+1:t,k}^d}{\partial \hat{z}_{t-\tau+1:t,i}^s} + \frac{\partial \log |J_h|}{\hat{z}_{t-\tau+1:t,i}^s}\end{aligned}\tag{B.33}$$

Then we further take the second-order derivative w.r.t  $z_{t-\tau,l}^d$ , where  $l \in \{1, \dots, n_s\}$  and we have:

$$\begin{aligned}\frac{\partial^2 \log p(\hat{z}_{t-\tau+1:t} | \mathbf{z}_{t-\tau}^d)}{\partial \hat{z}_{t-\tau+1:t,i}^s \partial z_{t-\tau,l}^d} &= \sum_{k=1}^{n_s} \frac{\partial^2 \log p(z_{t-\tau+1:t,k}^s | \mathbf{z}_{t-\tau}^d)}{\partial z_{t-\tau+1:t,k}^s \partial z_{t-\tau,l}^d} \cdot \frac{\partial z_{t-\tau+1:t,k}^s}{\partial \hat{z}_{t-\tau+1:t,i}^s} + \\ &\sum_{k=n_s+1}^n \frac{\partial^2 \log p(z_{t-\tau+1:t,k}^d | \mathbf{z}_{t-\tau}^d)}{\partial z_{t-\tau+1:t,k}^d \partial z_{t-\tau,l}^d} \cdot \frac{\partial z_{t-\tau+1:t,k}^d}{\partial \hat{z}_{t-\tau+1:t,i}^s} + \frac{\partial^2 \log |J_h|}{\partial \hat{z}_{t-\tau+1:t,i}^s \partial z_{t-\tau,l}^d}\end{aligned}\tag{B.34}$$

Since  $\frac{\partial^2 \log p(\hat{z}_{t-\tau+1:t} | \mathbf{z}_{t-\tau}^d)}{\partial \hat{z}_{t-\tau+1:t,i}^s}$  does not change across different values of  $z_{t-\tau,l}^d$ , then  $\frac{\partial^2 p(\hat{z}_{t-\tau+1:t} | \mathbf{z}_{t-\tau}^d)}{\partial \hat{z}_{t-\tau+1:t,i}^s \partial z_{t-\tau,l}^d} = 0$ . Moreover, since  $\frac{\partial^2 \log p(z_{t-\tau+1:t,k}^s | \mathbf{z}_{t-\tau}^d)}{\partial z_{t-\tau+1:t,k}^s \partial z_{t-\tau,l}^d}$  and  $\frac{\partial^2 \log |J_h|}{\partial \hat{z}_{t-\tau+1:t,i}^s \partial z_{t-\tau,l}^d} = 0$ , Equation (B.34) can be further rewritten as:

$$\sum_{k=n_s+1}^n \frac{\partial^2 \log p(z_{t-\tau+1:t,k}^d | \mathbf{z}_{t-\tau}^d)}{\partial z_{t-\tau+1:t,k}^d \partial z_{t-\tau,l}^d} \cdot \frac{\partial z_{t-\tau+1:t,k}^d}{\partial \hat{z}_{t-\tau+1:t,i}^s} = 0\tag{B.35}$$

By leveraging the linear independence assumption, the linear system denoted by Equation (B.35) has the only solution  $\frac{\partial z_{t-\tau+1:t,k}^d}{\partial \hat{z}_{t-\tau+1:t,i}^s} = 0$ . As  $h$  is smooth, its Jacobian can be written as:

$$\mathbf{J}_{h_z} = \left[ \begin{array}{c|c} \mathbf{A} := \frac{\partial \mathbf{z}_t^s}{\partial \hat{\mathbf{z}}_t^s} & \mathbf{B} := \frac{\partial \mathbf{z}_t^s}{\partial \hat{\mathbf{z}}_t^d} = 0 \\ \hline \mathbf{C} := \frac{\partial \mathbf{z}_t^d}{\partial \hat{\mathbf{z}}_t^s} = 0 & \mathbf{D} := \frac{\partial \mathbf{z}_t^d}{\partial \hat{\mathbf{z}}_t^d} \end{array} \right]\tag{B.36}$$

Therefore,  $\mathbf{z}_t^s$  and  $\mathbf{z}_t^d$  are subspace identifiable.  $\square$

### Evident Lower Bound

In this subsection, we show the evident lower bound. We first factorize the conditional distribution according to the Bayes theorem.

$$\begin{aligned}\ln p(\mathbf{x}_{1:H}) &= \ln \frac{p(\mathbf{z}_{1:H}^s, \mathbf{z}_{1:H}^d, \mathbf{x}_{1:H})}{p(\mathbf{z}_{1:H}^s, \mathbf{z}_{1:H}^d | \mathbf{x}_{1:H})} = \ln \frac{p(\mathbf{x}_{1:H} | \mathbf{z}_{1:H}^s, \mathbf{z}_{1:H}^d) p(\mathbf{z}_{1:H}^s, \mathbf{z}_{1:H}^d)}{p(\mathbf{z}_{1:H}^s, \mathbf{z}_{1:H}^d | \mathbf{x}_{1:H})} \\ &= \mathbb{E}_{q(\mathbf{z}_{1:H}^s, \mathbf{z}_{1:H}^d | \mathbf{x}_{1:H})} \ln \frac{p(\mathbf{x}_{1:H} | \mathbf{z}_{1:H}^s, \mathbf{z}_{1:H}^d) p(\mathbf{z}_{1:H}^s, \mathbf{z}_{1:H}^d) q(\mathbf{z}_{1:H}^s, \mathbf{z}_{1:H}^d | \mathbf{x}_{1:H})}{p(\mathbf{z}_{1:H}^s, \mathbf{z}_{1:H}^d | \mathbf{x}_{1:H}) q(\mathbf{z}_{1:H}^s, \mathbf{z}_{1:H}^d | \mathbf{x}_{1:H})} \\ &\geq \mathbb{E}_{q(\mathbf{z}_{1:H}^s, \mathbf{z}_{1:H}^d | \mathbf{x}_{1:H})} \ln p(\mathbf{x}_{1:H} | \mathbf{z}_{1:H}^s, \mathbf{z}_{1:H}^d) - D_{KL}(q(\mathbf{z}_{1:H}^s, \mathbf{z}_{1:H}^d | \mathbf{x}_{1:H}) || p(\mathbf{z}_{1:H}^s, \mathbf{z}_{1:H}^d))\end{aligned}\tag{B.37}$$

specifically:

$$\ln \frac{p(\mathbf{x}_{1:H} | \mathbf{z}_{1:H}^s, \mathbf{z}_{1:H}^d) p(\mathbf{z}_{1:H}^s, \mathbf{z}_{1:H}^d)}{p(\mathbf{z}_{1:H}^s, \mathbf{z}_{1:H}^d | \mathbf{x}_{1:H})} = \ln \frac{p(\mathbf{x}_{1:H} | \mathbf{z}_{1:H}^s, \mathbf{z}_{1:H}^d) p(\mathbf{z}_{1:H}^s | \mathbf{z}_{1:H}^d) p(\mathbf{z}_{1:H}^d)}{p(\mathbf{z}_{1:H}^s, \mathbf{z}_{1:H}^d | \mathbf{x}_{1:H})} \quad (\text{B.38})$$

In the absence of  $x_t$ ,  $z_t^d$  and  $z_t^s$  are independent. So the original expression is equal to:

$$\begin{aligned} &= \ln \frac{p(\mathbf{x}_{1:H} | \mathbf{z}_{1:H}^s, \mathbf{z}_{1:H}^d) p(\mathbf{z}_{1:H}^s) p(\mathbf{z}_{1:H}^d)}{p(\mathbf{z}_{1:H}^s, \mathbf{z}_{1:H}^d | \mathbf{x}_{1:H})} = \ln \frac{p(\mathbf{x}_{1:H} | \mathbf{z}_{1:H}^s, \mathbf{z}_{1:H}^d) p(\mathbf{z}_{1:H}^s) p(\mathbf{z}_{1:H}^d) q(\mathbf{z}_{1:H}^s | \mathbf{x}_{1:H}) q(\mathbf{z}_{1:H}^d | \mathbf{x}_{1:H})}{p(\mathbf{z}_{1:H}^s, \mathbf{z}_{1:H}^d | \mathbf{x}_{1:H}) q(\mathbf{z}_{1:H}^s | \mathbf{x}_{1:H}) q(\mathbf{z}_{1:H}^d | \mathbf{x}_{1:H})} \\ &\geq \mathbb{E}_{q(\mathbf{z}_{1:H}^s | \mathbf{x}_{1:H})} \mathbb{E}_{q(\mathbf{z}_{1:H}^d | \mathbf{x}_{1:H})} \ln p(\mathbf{x}_{1:H} | \mathbf{z}_{1:H}^s, \mathbf{z}_{1:H}^d) - D_{KL}(q(\mathbf{z}_{1:H}^s | \mathbf{x}_{1:H}) || p(\mathbf{z}_{1:H}^s)) \\ &\quad - D_{KL}(q(\mathbf{z}_{1:H}^d | \mathbf{x}_{1:H}) || p(\mathbf{z}_{1:H}^d)) \end{aligned}$$

### Prior Likelihood Derivation

In this section, we derive the prior (As an example, for  $z^s$ ) of  $p(\hat{\mathbf{z}}_{1:t}^s)$  and  $p(\hat{\mathbf{z}}_{1:t}^d)$  as follows: We consider the prior of  $\ln p(\mathbf{z}_{1:t}^s)$ . We start with an illustrative example of long/short-term latent causal processes with two time-delay latent variables, i.e.  $\mathbf{z}_t^s = [z_{t,1}^s, z_{t,2}^s]$  with maximum time lag  $L = 1$ , i.e.,  $z_{t,i}^s = f_i(\mathbf{z}_{t-1}^s, \epsilon_{t,i}^s)$  with mutually independent noises. Then we write this latent process as a transformation map  $\mathbf{f}$  (note that we overload the notation  $f$  for transition functions and for the transformation map):

$$\begin{bmatrix} z_{t-1,1}^s \\ z_{t-1,2}^s \\ z_{t,1}^s \\ z_{t,2}^s \end{bmatrix} = \mathbf{f} \left( \begin{bmatrix} z_{t-1,1}^s \\ z_{t-1,2}^s \\ \epsilon_{t,1}^s \\ \epsilon_{t,2}^s \end{bmatrix} \right).$$

By applying the change of variables formula to the map  $\mathbf{f}$ , we can evaluate the joint distribution of the latent variables  $p(z_{t-1,1}^s, z_{t-1,2}^s, z_{t,1}^s, z_{t,2}^s)$  as

$$p(z_{t-1,1}^s, z_{t-1,2}^s, z_{t,1}^s, z_{t,2}^s) = \frac{p(z_{t-1,1}^s, z_{t-1,2}^s, \epsilon_{t,1}^s, \epsilon_{t,2}^s)}{|\det \mathbf{J}_f|}, \quad (\text{B.39})$$

where  $\mathbf{J}_f$  is the Jacobian matrix of the map  $\mathbf{f}$ , which is naturally a low-triangular matrix:

$$\mathbf{J}_f = \begin{bmatrix} 1 & 0 & 0 & 0 \\ 0 & 1 & 0 & 0 \\ \frac{\partial z_{t,1}^s}{\partial z_{t-1,1}^s} & \frac{\partial z_{t,1}^s}{\partial z_{t-1,2}^s} & \frac{\partial z_{t,1}^s}{\partial \epsilon_{t,1}^s} & 0 \\ \frac{\partial z_{t,2}^s}{\partial z_{t-1,1}^s} & \frac{\partial z_{t,2}^s}{\partial z_{t-1,2}^s} & 0 & \frac{\partial z_{t,2}^s}{\partial \epsilon_{t,2}^s} \end{bmatrix}.$$

Given that this Jacobian is triangular, we can efficiently compute its determinant as  $\prod_i \frac{\partial z_{t,i}^s}{\partial \epsilon_{t,i}^s}$ . Furthermore, because the noise terms are mutually independent, and hence  $\epsilon_{t,i}^s \perp \epsilon_{t,j}^s$  for  $j \neq i$  and  $\epsilon_t^s \perp \mathbf{z}_{t-1}^s$ , so we can with the RHS of Equation (B.39) as follows:

$$p(z_{t-1,1}^s, z_{t-1,2}^s, z_{t,1}^s, z_{t,2}^s) = p(z_{t-1,1}^s, z_{t-1,2}^s) \times \frac{p(\epsilon_{t,1}^s, \epsilon_{t,2}^s)}{|\mathbf{J}_f|} = p(z_{t-1,1}^s, z_{t-1,2}^s) \times \frac{\prod_i p(\epsilon_{t,i}^s)}{|\mathbf{J}_f|}. \quad (\text{B.40})$$

Finally, we generalize this example and derive the prior likelihood below. Let  $\{r_i^s\}_{i=1,2,3,\dots}$  be a set of learned inverse transition functions that take the estimated latent causal variables, and output the noise terms, i.e.,  $\hat{\epsilon}_{t,i}^s = r_i^s(\hat{\mathbf{z}}_{t,i}^s, \{\hat{\mathbf{z}}_{t-\tau}^s\})$ . Then we design a transformation  $\mathbf{A} \rightarrow \mathbf{B}$  with low-triangular Jacobian as follows:

$$\underbrace{[\hat{\mathbf{z}}_{t-L}^s, \dots, \hat{\mathbf{z}}_{t-1}^s, \hat{\mathbf{z}}_t^s]^\top}_{\mathbf{A}} \text{ mapped to } \underbrace{[\hat{\mathbf{z}}_{t-L}^s, \dots, \hat{\mathbf{z}}_{t-1}^s, \hat{\epsilon}_{t,i}^s]^\top}_{\mathbf{B}}, \text{ with } \mathbf{J}_{\mathbf{A} \rightarrow \mathbf{B}} = \begin{bmatrix} \mathbb{I}_{n_s \times L} & 0 \\ * & \text{diag} \left( \frac{\partial r_i^s}{\partial \hat{\mathbf{z}}_{t,i}^s} \right) \end{bmatrix}. \quad (\text{B.41})$$

Similar to Equation (B.40), we can obtain the joint distribution of the estimated dynamics subspace as:

$$\log p(\mathbf{A}) = \log p(\hat{\mathbf{z}}_{t-L}^s, \dots, \hat{\mathbf{z}}_{t-1}^s) + \underbrace{\sum_{i=1}^{n_s} \log p(\hat{\epsilon}_{t,i}^s) + \log(|\det(\mathbf{J}_{\mathbf{A} \rightarrow \mathbf{B}})|)}_{\text{Because of mutually independent noise assumption}} \quad (\text{B.42})$$

Finally, we have:

$$\log p(\hat{\mathbf{z}}_t^s | \{\hat{\mathbf{z}}_{t-\tau}^s\}_{\tau=1}^L) = \sum_{i=1}^{n_s} \log p(\hat{\epsilon}_{t,i}^s) + \sum_{i=1}^{n_s} \log \left| \frac{\partial r_i^s}{\partial \hat{\mathbf{z}}_{t,i}^s} \right| \quad (\text{B.43})$$

Since the prior of  $p(\hat{\mathbf{z}}_{t+1:T}^s | \hat{\mathbf{z}}_{1:t}^s) = \prod_{i=t+1}^T p(\hat{\mathbf{z}}_i^s | \hat{\mathbf{z}}_{i-1}^s)$  with the assumption of first-order Markov assumption, we can estimate  $p(\hat{\mathbf{z}}_{t+1:T}^s | \hat{\mathbf{z}}_{1:t}^s)$  in a similar way.

Table 3: Architecture details. H: length of time series, L: length of observed time series, LeakyReLU: Leaky Rectified Linear Unit,  $|x_t|$  : the dimension of  $x_t$

Configuration	Description	Output
1. $\phi^s$	Long-term Variable Encoder	
Input $\mathbf{x}_{1:L}$	Observed time series	$BatchSize \times L \times  \mathbf{x}_t $
Dense	Conv1d	$BatchSize \times 640 \times  \mathbf{x}_t $
Dense	L neurons; LeakyReLU	$BatchSize \times L \times  \mathbf{x}_t $
2. $\phi^d$	Short-term Variable Encoder	
Input $\mathbf{x}_{1:L}$	Observed time series	$BatchSize \times L \times  \mathbf{x}_t $
Dense	512 neurons; LeakyReLU	$BatchSize \times 512 \times  \mathbf{x}_t $
Dense	L neurons; LeakyReLU	$BatchSize \times L \times  \mathbf{x}_t $
3. $T^s$	Long-term Variable Predict Module	
Input $\mathbf{z}_{1:L}^s$	Long-term Latent Variables	$BatchSize \times L \times  \mathbf{x}_t $
Dense	512 neurons; LeakyReLU	$BatchSize \times 512 \times  \mathbf{x}_t $
Dense	(H-L) neurons; LeakyReLU	$BatchSize \times (H - L) \times  \mathbf{x}_t $
4. $T^d$	Short-term Variable Predict Module	
Input $\mathbf{z}_{1:L}^d$	Long-term Latent Variables	$BatchSize \times L \times  \mathbf{x}_t $
Dense	(H-L) neurons; LeakyReLU	$BatchSize \times (H - L) \times  \mathbf{x}_t $
5. $F_x$	Historical Decoder	
Input $\mathbf{z}_{1:L}^s, \mathbf{z}_{1:L}^d$	Long/Short-term Latent Variable concatenation	$BatchSize \times L \times  \mathbf{x}_t , BatchSize \times L \times  \mathbf{x}_t $
Concat		$BatchSize \times L \times 2 \mathbf{x}_t $
Dense	$ \mathbf{x}_t $ neurons; LeakyReLU	$BatchSize \times L \times  \mathbf{x}_t $
6. $F_y$	Future Predictor	
Input $\mathbf{z}_{L+1:H}^s, \mathbf{z}_{L+1:H}^d$	Long/Short-term Latent Variable concatenation	$BatchSize \times (H - L) \times  \mathbf{x}_t , BatchSize \times (H - L) \times  \mathbf{x}_t $
Concat		$BatchSize \times (H - L) \times 2 \mathbf{x}_t $
Dense	512 neurons; LeakyReLU	$BatchSize \times (H - L) \times 512$
Dense	$ \mathbf{x}_t $ neurons; LeakyReLU	$BatchSize \times (H - L) \times  \mathbf{x}_t $
7. $r$	Modular Prior Networks	
Input $\mathbf{z}_{1:L}^s$ or $\mathbf{z}_{1:L}^d$	Latent Variables	$BatchSize \times (n_* + 1)$
Dense	128 neurons, LeakyReLU	$(n_* + 1) \times 128$
Dense	128 neurons, LeakyReLU	$128 \times 128$
Dense	128 neurons, LeakyReLU	$128 \times 128$
JacobianCompute	Compute log (det (J))	$BatchSize$

## C. Implementation Details

### Model Details

We choose FSNet (Pham et al. 2022) as the encoder backbone of long latent variables and MLP as the encoder backbone of short latent variables. Specifically, given the FSNet and MLP extract the hidden feature,  $z_t^d$  and  $z_t^s$ , we apply a variational inference block and then a MLP-based decoder. Meanwhile, inspired by OneNet (Wen et al. 2024), we introduce a hyperparameter “mode” to choose between feature-based and time-based to extraction extract the hidden feature. Architecture details of the proposed method are shown in Table3

### Experiment Details.

We use ADAM optimizer in all experiments and report the mean squared error (MSE) and the mean absolute error (MAE) as evaluation metrics. All experiments are implemented by Pytorch on a single NVIDIA GTX 3090 24GB GPU.

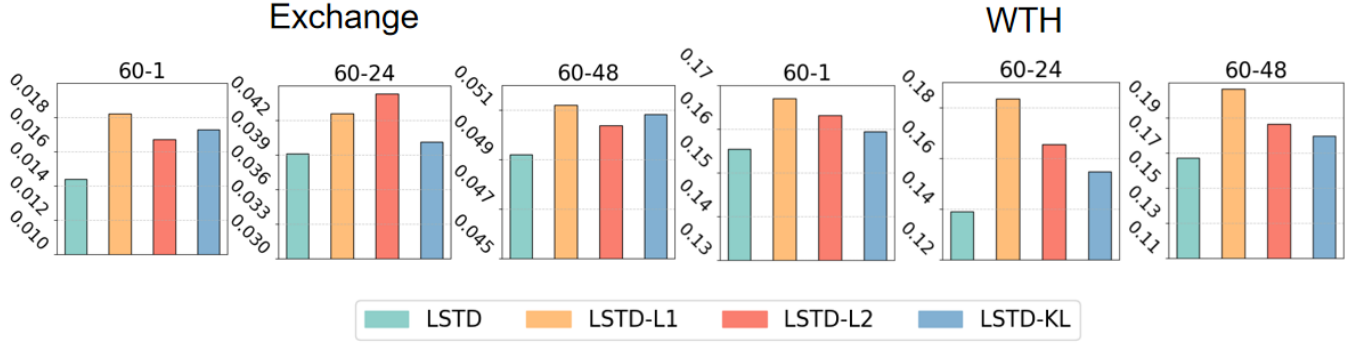


Figure 5: All ablation experiments

Table 4: Experiments results on the Exchange data with different input horizons

Length	20-24		30-24		40-24		50-24		60-24	
	Method	MSE	MAE	MSE	MAE	MSE	MAE	MSE	MAE	MSE
LSTD	<b>0.043</b>	<b>0.138</b>	<b>0.046</b>	<b>0.144</b>	<b>0.044</b>	<b>0.141</b>	<b>0.039</b>	<b>0.132</b>	<b>0.039</b>	<b>0.132</b>
OneNet	0.048	0.148	0.049	0.152	0.048	0.147	0.049	0.15	0.047	0.148
FSNet	0.133	0.223	0.125	0.210	0.141	0.216	0.125	0.208	0.113	0.206
OneNet-T	0.063	0.168	0.059	0.164	0.059	0.164	0.064	0.166	0.060	0.166
DER++	0.138	0.231	0.127	0.237	0.149	0.234	0.121	0.229	0.111	0.227
ER	0.183	0.218	0.178	0.22	0.188	0.225	0.174	0.212	0.162	0.210
MIR	0.122	0.204	0.115	0.210	0.119	0.207	0.113	0.207	0.104	0.204
TFCL	0.106	0.239	0.110	0.246	0.106	0.233	0.103	0.241	0.098	0.227
Online-T	0.134	0.217	0.128	0.231	0.137	0.224	0.122	0.221	0.116	0.213
Informer	0.123	0.237	0.134	0.231	0.117	0.229	0.121	0.224	0.107	0.196

## D. More Experiments Results

### Ablation Study

In the main text, we conducted three ablation experiments. All ablation experiments are shown in the figure 5. It can be shown in Table 4 that our model can adapt to the nonstationary data with few samples. We can find that even if the input horizon is small, e.g. 20, our method can successfully adapt to the nonstationary data with few samples.

### Model Efficiency

We evaluate the performance of our model and the baseline model on the exchange rate dataset from three aspects: forecasting performance, training speed, and memory footprint as shown in Figure 6. Compared with other models for online time-series forecasting, we can find that the proposed **LSTD** has the best model performance and relatively good model efficiency. However, in terms of memory performance, **LSTD** may be lower than other baselines because we need to incorporate priors during the training process.

### Experiments of Real-world Datasets

In the main text, to ensure the reproducibility of other baselines, we used the tabular data from the OneNet(Wen et al. 2024). For the sake of fairness, we also ran the experiment three times on the same machine with seeds 2023, 2024, 2025. And we recorded the mean and variance of all methods. The results can be seen in Table 5 to Table 8. The complete visualization in the Weather dataset is shown in Figure 7.

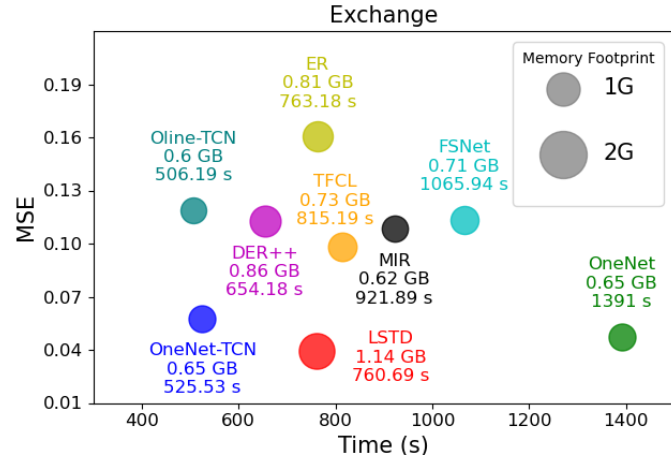


Figure 6: Model efficiency comparison of different methods. Training time and memory footprint are recorded with the same batch size and official configuration.

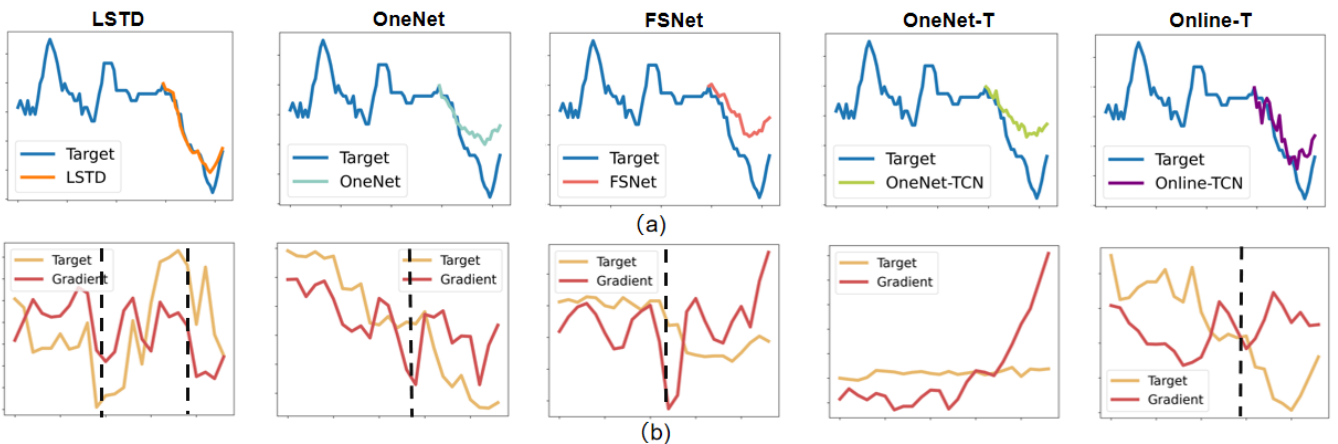


Figure 7: The figure represents visualization of the proposed LSTD and other baselines. The blue lines denote the ground-truth time series data and the lines with other colors denote the predicted results of different methods.

Table 5: Mean Square Error (MSE) results on the different datasets with three different seeds. TCN is abbreviated as T

Models	Len	LSTD	OneNet	FSNet	OneNet-T	DER++	ER	MIR	TFCL	Online-T	Informer
ETTh2	1	<b>0.375</b>	0.377	0.491	0.394	0.511	0.581	0.524	0.531	0.617	8.126
	24	<b>0.543</b>	0.548	0.768	0.943	0.836	0.802	0.816	0.851	0.832	5.173
	48	<b>0.616</b>	0.622	0.948	0.926	1.157	1.103	1.098	1.211	1.188	6.272
ETTm1	1	<b>0.082</b>	0.086	0.093	0.091	0.082	0.089	0.082	0.085	0.208	0.443
	24	<b>0.102</b>	0.105	0.195	0.213	0.198	0.205	0.189	0.216	0.263	0.465
	48	0.115	<b>0.110</b>	0.185	0.216	0.203	0.231	0.223	0.240	0.271	0.391
WTH	1	<b>0.155</b>	0.157	0.167	0.157	0.172	0.182	0.182	0.176	0.213	0.422
	24	<b>0.139</b>	0.173	0.177	0.276	0.279	0.290	0.286	0.311	0.312	0.376
	48	<b>0.167</b>	0.196	0.193	0.289	0.233	0.301	0.289	0.324	0.298	0.384
ECL	1	<b>2.228</b>	2.675	3.586	2.413	2.692	2.618	2.568	2.806	3.312	3.813
	24	<b>1.557</b>	2.090	6.055	4.551	8.961	9.235	9.157	11.891	11.594	9.185
	48	<b>1.720</b>	2.438	7.881	4.488	8.994	9.597	9.391	12.109	11.912	10.183
Traffic	1	<b>0.234</b>	0.241	0.312	0.236	0.271	0.284	0.298	0.306	0.334	0.234
	24	<b>0.417</b>	0.438	0.426	0.425	0.476	0.461	0.451	0.441	0.481	0.451
	48	<b>0.431</b>	0.473	0.445	0.451	0.486	0.510	0.502	0.438	0.503	0.496
Exchange	1	<b>0.014</b>	0.017	0.094	0.031	0.106	0.097	0.095	0.106	0.113	0.102
	24	<b>0.039</b>	0.047	0.113	0.060	0.111	0.162	0.104	0.098	0.116	0.107
	48	<b>0.049</b>	0.062	0.156	0.065	0.183	0.181	0.101	0.101	0.168	0.116

Table 6: Mean Absolute Error (MAE) results on the different datasets with three different seeds. TCN is abbreviated as T

Models	Len	LSTD	OneNet	FSNet	OneNet-T	DER++	ER	MIR	TFCL	Online-T	Informer
ETTh2	1	<b>0.347</b>	0.354	0.471	0.373	0.373	0.381	0.418	0.466	0.443	0.852
	24	<b>0.411</b>	0.415	0.557	0.532	0.536	0.515	0.543	0.539	0.545	0.652
	48	<b>0.423</b>	0.448	0.541	0.535	0.579	0.586	0.572	0.591	0.598	0.768
ETTm1	1	<b>0.189</b>	0.192	0.244	0.207	0.196	0.208	0.201	0.192	0.218	0.510
	24	<b>0.217</b>	0.234	0.326	0.343	0.331	0.343	0.327	0.346	0.376	0.518
	48	0.259	<b>0.242</b>	0.319	0.348	0.356	0.367	0.347	0.357	0.415	0.462
WTH	1	<b>0.200</b>	0.202	0.224	0.206	0.176	0.182	0.182	0.169	0.210	0.438
	24	<b>0.224</b>	0.255	0.261	0.337	0.304	0.284	0.317	0.314	0.317	0.380
	48	<b>0.250</b>	0.277	0.276	0.354	0.300	0.296	0.289	0.325	0.334	0.361
ECL	1	<b>0.232</b>	0.268	0.545	0.280	0.428	0.518	0.519	0.273	0.641	0.549
	24	<b>0.288</b>	0.341	1.116	0.405	1.081	1.184	1.035	1.194	1.291	1.098
	48	<b>0.348</b>	0.367	1.194	0.423	1.054	1.031	1.184	1.304	1.219	1.164
Traffic	1	<b>0.229</b>	0.240	0.278	0.236	0.251	0.256	0.284	0.297	0.284	0.258
	24	<b>0.332</b>	0.346	0.365	0.346	0.409	0.417	0.443	0.493	0.385	0.365
	48	<b>0.344</b>	0.371	0.378	0.355	0.386	0.294	0.397	0.531	0.380	0.394
Exchange	1	<b>0.070</b>	0.085	0.174	0.117	0.173	0.124	0.118	0.153	0.169	0.115
	24	<b>0.132</b>	0.148	0.206	0.166	0.227	0.210	0.204	0.227	0.213	0.196
	48	<b>0.150</b>	0.170	0.254	0.173	0.243	0.241	0.209	0.183	0.258	0.217

Table 7: Standard deviation of MSE results on the different datasets

Models	Len	LSTD	OneNet	FSNet	OneNet-T	DER++	ER	MIR	TFCL	Online-T	Informer
ETTh2	1	6.05e-04	7.29e-05	3.43e-01	5.74e-05	2.65e-03	1.72e-02	1.51e-02	3.33e-02	2.23e-04	2.59e-03
	24	6.79e-04	1.87e-04	7.85e-01	2.44e-02	2.21e-02	3.17e-03	2.62e-02	4.89e-03	9.52e-05	1.52e-03
	48	8.70e-04	6.92e-04	8.84e-03	6.87e-03	1.45e-02	2.74e-03	6.84e-03	1.74e-02	2.94e-04	1.29e-03
ETTm1	1	9.35e-07	6.26e-06	1.69e-03	7.26e-05	1.75e-03	8.90e-03	1.91e-02	1.58e-02	8.73e-05	1.71e-04
	24	1.05e-07	3.10e-06	6.37e-04	6.10e-06	1.75e-02	2.69e-02	1.23e-02	2.70e-02	6.35e-05	2.52e-04
	48	2.46e-04	1.45e-06	4.66e-04	4.67e-05	1.27e-02	2.44e-02	1.37e-03	5.83e-03	2.01e-04	1.43e-03
WTH	1	7.15e-07	3.81e-07	8.82e-07	2.38e-07	1.44e-02	2.19e-02	3.05e-02	1.54e-02	2.61e-04	1.86e-04
	24	5.45e-06	6.76e-06	3.50e-06	5.44e-06	1.01e-02	1.18e-02	1.47e-02	3.18e-02	2.78e-04	3.02e-04
	48	3.07e-05	1.69e-05	1.11e-05	1.01e-04	1.14e-03	2.15e-02	1.79e-02	3.20e-02	1.17e-04	8.04e-05
ECL	1	3.87e-04	2.02e-03	3.17e-02	1.18e-03	2.90e-03	3.06e-04	1.42e-04	6.65e-03	2.32e-04	1.60e-03
	24	6.57e-04	4.19e-04	2.39e-01	1.06e-03	1.43e-04	1.67e-04	2.56e-05	1.07e-04	3.17e-04	3.25e-03
	48	4.26e-02	1.00e-02	4.15e-01	2.30e-04	2.27e-02	3.27e-04	1.58e-04	6.49e-05	8.39e-05	1.54e-04
Traffic	1	7.33e-06	1.06e-06	9.96e-06	2.30e-06	1.14e-04	6.80e-05	2.21e-04	2.67e-05	2.14e-03	2.42e-04
	24	4.89e-05	4.59e-05	2.70e-05	2.13e-05	3.87e-03	1.35e-04	2.18e-04	1.06e-04	1.80e-04	1.19e-04
	48	5.93e-06	8.38e-04	6.02e-05	2.22e-06	9.09e-05	1.16e-04	2.52e-04	3.05e-04	3.23e-04	6.74e-05
Exchange	1	2.85e-07	1.22e-06	8.55e-04	4.23e-06	1.68e-05	3.50e-05	1.69e-04	2.49e-04	7.35e-05	2.12e-04
	24	1.66e-08	4.10e-05	2.13e-04	9.82e-07	5.92e-05	2.40e-04	4.92e-05	1.92e-04	1.88e-04	5.37e-05
	48	2.95e-06	2.91e-04	1.35e-04	4.79e-06	7.38e-05	4.58e-05	1.47e-05	1.59e-04	4.48e-05	1.81e-04

Table 8: Standard deviation of MAE results on the different datasets

Models	Len	LSTD	OneNet	FSNet	OneNet-T	DER++	ER	MIR	TFCL	Online-T	Informer
ETTh2	1	5.38e-05	2.86e-05	3.38e-04	4.41e-05	1.96e-03	7.04e-05	1.70e-04	3.34e-04	3.08e-04	1.26e-04
	24	9.95e-06	3.71e-05	1.23e-03	3.02e-04	1.92e-03	2.35e-04	1.66e-03	2.21e-03	4.39e-05	3.15e-05
	48	3.66e-05	9.72e-05	5.46e-05	1.56e-04	1.92e-04	3.07e-05	9.69e-05	1.35e-05	1.33e-04	6.90e-05
ETTm1	1	4.62e-06	2.06e-05	1.61e-03	1.51e-04	3.02e-03	1.63e-04	2.05e-04	2.67e-03	3.06e-04	2.17e-04
	24	6.97e-08	4.91e-06	5.10e-04	4.02e-06	2.23e-03	6.26e-05	2.76e-03	3.26e-04	2.27e-05	6.31e-05
	48	1.38e-04	1.44e-06	4.31e-04	3.80e-05	1.23e-03	6.94e-05	7.37e-05	3.19e-03	1.59e-04	2.96e-04
WTH	1	1.11e-06	2.58e-07	1.90e-06	2.00e-07	2.30e-03	2.60e-05	8.26e-05	2.65e-04	6.14e-05	1.28e-03
	24	1.07e-06	7.48e-06	4.08e-06	5.36e-06	3.05e-03	1.06e-04	6.12e-05	8.00e-05	2.46e-04	2.12e-06
	48	1.94e-05	1.50e-05	8.51e-06	2.48e-05	3.03e-03	2.99e-04	1.75e-04	3.38e-04	4.01e-05	2.84e-04
ECL	1	3.05e-05	1.58e-06	2.62e-04	1.99e-05	9.00e-04	1.12e-04	7.17e-05	3.30e-03	1.63e-06	2.16e-04
	24	1.91e-05	6.26e-06	1.79e-04	1.20e-08	1.36e-03	2.35e-05	3.38e-03	3.09e-04	2.31e-04	3.89e-05
	48	4.71e-03	2.19e-05	1.95e-04	1.60e-06	1.20e-03	5.26e-05	1.56e-04	3.16e-05	3.21e-04	1.78e-03
Traffic	1	7.73e-06	3.32e-07	7.15e-06	2.02e-06	7.03e-04	1.49e-04	5.18e-05	1.56e-04	1.11e-04	2.21e-04
	24	1.79e-05	7.31e-06	1.71e-05	7.16e-06	3.78e-04	1.88e-04	1.13e-04	2.25e-04	3.30e-04	7.38e-05
	48	4.36e-06	2.08e-04	3.21e-05	1.72e-06	2.92e-04	2.11e-04	7.86e-06	2.71e-04	2.79e-06	1.60e-04
Exchange	1	3.24e-06	9.36e-06	6.65e-04	1.13e-05	1.34e-05	2.93e-05	8.01e-05	1.01e-06	2.97e-04	8.06e-05
	24	1.66e-08	9.11e-05	8.26e-05	1.93e-06	1.26e-05	1.12e-04	1.94e-04	2.59e-05	1.55e-06	2.13e-04
	48	1.06e-05	5.79e-04	1.08e-04	9.63e-06	8.39e-06	1.86e-04	1.86e-06	3.01e-04	3.05e-08	3.42e-04